COMPARISON AND ANALYSIS OF SOME NUMERICAL SCHEMES FOR STIFF COMPLEX CHEMISTRY PROBLEMS

Yves D'Angelo[1] – Bernard Larrouturou
CERMICS, INRIA, B.P. 93, 06902 Sophia–Antipolis Cedex

Abstract

Considering the finite-volume solution of multi-dimensional multi-species reactive flows with complex chemistry, we concentrate on the numerical treatment of the chemical source terms in a fractional step approach. For two air-hydrogen chemistry models, we compare the numerical efficiency of linearized or totally implicit schemes, in both temperature-mass-fractions coupled and uncoupled formulations; we also use two popular specialized solvers, LSODE and DASSL. The implicit schemes suffer from very drastic stability criteria; they may even become unconditionaly unstable for some particular initial conditions. Analysing several simplified models, we explain these instabilities. In particular, we show why the linearized implicit methods, which are perfectly adequate for globally endothermic complex chemistries, are limited in an exothermic situation by a stabilty condition which may even be worse than the stability criterion of an explicit scheme.

COMPARAISON ET ANALYSE DE SCHEMAS NUMERIQUES POUR LA RESOLUTION DE PROBLEMES DE CINETIQUE CHIMIQUE COMPLEXE RAIDE

Résumé

On s'intéresse à la résolution par des méthodes de volumes finis décentrées des équations d'Euler multi-dimensionnelles et multi-espèces, comportant en outre des termes sources chimiques. Nous concentrant sur le traitement des termes de réaction, nous comparons pour deux chimies air-hydrogène l'efficacité numérique de schémas implicites, linéarisés ou non, avec plusieurs formulations qui couplent ou découplent partiellement la température et les fractions massiques; nous utilisons également deux solveurs spécialisés, LSODE et DASSL. Les schémas implicites s'avèrent très instables, voire inconditionnellement instables pour certaines conditions initiales. En analysant ensuite quelques modèles simplifiés, nous expliquons ces instabilités. En particulier, nous montrons pourquoi les méthodes implicites linéarisées, qui s'avèrent efficaces pour des chimies complexes globalement endothermiques, souffrent dans le cas de chimies exothermiques de conditions de stabilité qui peuvent même être plus sévères que celle d'un schéma explicite.

[1]This author was supported by DRET under contract 92-1575A.

1 Introduction

Numerical solution of inviscid flows is now quite achievable: a good deal of efficient algorithms have appeared which make possible to solve the Euler equations of motion for most practical cases. For chemically reactive flows however, severe numerical difficulties may arise from the introduction of the highly non-linear chemical source terms – in particular when the number of species and of reactions is large – which generally lead to very stiff systems of differential equations.

In the case of hypersonic flows, the decomposition of the molecules of air (N_2 and O_2) only occur at very high temperature and the chemical phenomenon is globally endothermic. For this kind of chemical kinetics, a linearized implicit treatment of the chemical terms seems to be sufficiently efficient to solve the flow and does not affect the C.F.L. condition by more than a factor of two, even in the case of a complex chemistry model with 5 species and 18 reactions [2, 3, 8]. The extension of this method to a globally exothermic kinetic model, such as the models arising in combustion, seems to lead to a very different – and highly unstable ! – behaviour for this kind of linearized implicit methods. Moreover, numerical instability may sometimes appear even when non-linearized implicit methods are applied.

It is precisely the aim of our work to investigate how implicit schemes behave and perform when applied to kinetic models arising from complex chemical mechanisms. Indeed, although our ultimate objective is the solution of multi-dimensional reactive flows, we will concentrate here on the treatment of the reaction terms in a fractional step approach. After having briefly presented the flow equations, we will focus on the integration of the chemical source terms, which we will describe in detail in the next section. Then, we will describe various numerical methods, whose behaviours will be discussed and compared by examining three numerical experiments, for two models of the hydrogen-air combustion. These methods include the explicit Euler forward scheme, an explicit second-order Runge-Kutta scheme, linearized or nonlinear implicit schemes, with two formulations coupling or uncoupling the temperature and mass fractions, and two specialized O.D.E. solvers (LSODE and DASSL). The last section is then devoted to the numerical analysis of the linearized implicit schemes, for several simpler kinetic mechanisms, including a one-step reversible equation and two global reversible one-reaction models for the hydrogen-air combustion. In particular, these analyses will show why the linearized implicit schemes are adequate for endothermic regimes (typically for the air chemistry, in hypersonic re-entry flows), while they encounter extremely severe stability restrictions in exothermic situations, such as those arising in combustion.

2 Governing equations

2.1 The two-dimensional reactive Euler equations

We are interested in the numerical simulation of multi-dimensional high-speed reactive flows, such as those occuring in hypersonics, supersonic combustion or detonations. Neglecting therefore the viscous and diffusive effects, we start from the following conservative form of the κ-components two-dimensional "reactive Euler" equations: given by :

$$\left\{ \begin{array}{l} (\rho_k)_t + (\rho_k u)_x + (\rho_k v)_y = \Omega_k(T, Y, \rho) \ , \\ (\rho u)_t + (\rho u^2 + P)_x + (\rho uv)_y = 0 \ , \\ (\rho v)_t + (\rho uv)_x + (\rho v^2 + P)_y = 0 \ , \\ e_t + (u(e+P))_x + (v(e+P))_y = 0 \ , \end{array} \right. \tag{1}$$

with $\rho_k = \rho Y_k$, Y_k being the mass fraction of species χ_k and Y the vector of the Y_k's; Ω_k is the chemical source term for the k-th species. The other notations are usual.

To close the system, we write two additional equations. The first one is the perfect gas law:

$$P = \sum_{k=1}^{\kappa} \rho_k \frac{RT}{M_k} \ , \tag{2}$$

and the second one is the equation of state giving the energy:

$$e = \frac{1}{2}\rho(u^2 + v^2) + \rho h(T, \rho_k) - P \ . \tag{3}$$

We will be more specific later about the precise form of the specific enthalpy $h(T, \rho_k)$ for the κ-components real-gas mixture.

We can also write the system in its classical vector form:

$$W_t + F(W)_x + G(W)_y + H(W) = 0 \ , \tag{4}$$

with:

$$W = \begin{pmatrix} \rho_k \\ \rho u \\ \rho v \\ e \end{pmatrix}, \ F(W) = \begin{pmatrix} \rho_k u \\ \rho u^2 + P \\ \rho uv \\ u(e+P) \end{pmatrix}, \ G(W) = \begin{pmatrix} \rho_k v \\ \rho uv \\ \rho v^2 + P \\ v(e+P) \end{pmatrix}, \ H(W) = \begin{pmatrix} -\Omega_k \\ 0 \\ 0 \\ 0 \end{pmatrix}. \tag{5}$$

We consider the solution of system (4) using semi-implicit upwind finite-volume methods. Semi-implicit means here that the convective (i.e., non reactive) part of the system is solved using a cheap explicit solver, whereas the reactive terms are integrated point-wise with a (preferably) implicit method. We write the global scheme as:

$$\mathcal{A}rea(C_i)\frac{W_i^{n+1} - W_i^n}{\Delta t} + \sum_{j \in \Lambda_i} \phi_{ij}(W_i^n, W_j^n, \vec{\eta}_{ij}) + \frac{\mathcal{A}rea(C_i)}{\Delta t}\int_{t^n}^{t^{n+1}} H(W_i(t))dt = 0 \ . \tag{6}$$

Here, the superscripts n and $n+1$ refer to the number of time steps, Δt is the time step, $\mathcal{A}rea(C_i)$ is the value of the area of the cell C_i, Λ_i is the set of neighbour nodes of vertex i, Lastly, ϕ_{ij} is the numerical flux between cells C_i and C_j; it depends on the two states W_i^n and W_j^n and on the integrated normal on the cell interface $\vec{\eta}_{ij} = \int_{C_i \cap C_j} \vec{\nu_i} \ d\sigma$. We evaluate these numerical fluxes for the real-gas mixture using an explicit second-order accurate multi-component Riemann solver, which has the property of preserving the maximum principle for the mass fractions. We refer to e.g. [1, 7] for a complete description of such numerical methods.

To be more specific, we have to consider the different possible ways of evaluating the integral $\int_{t^n}^{t^{n+1}} H(W_i(t))dt$. For instance, if we wimply set $\int_{t^n}^{t^{n+1}} H(W_i(t))dt = \Delta t H(W_i^n)$, we obtain a fully explicit scheme. But the timestep limitation for such an explicit scheme is usually very drastic in the presence of complex chemistry. This is why we have to consider semi-implicit schemes. On the other hand, writing $\int_{t^n}^{t^{n+1}} H(W_i(t))dt = \Delta t H(W_i^{n+1})$ leads to a nonlinear system in which all variables (at all nodes) are fully coupled. In order to avoid the cost of such an approach, we will consider instead a fractional step method, where the fluid–mechanics and the reactive part of the system are solved separately. We write the two steps as:

$$\begin{cases} \mathcal{A}rea(C_i)\dfrac{\bar{W}_i^{n+1} - W_i^n}{\Delta t} + \displaystyle\sum_{j \in \Lambda_i} \phi_{ij}(W_i^n, W_j^n, \vec{\eta}_{ij}) = 0 \ , \\ W_i^{n+1} - \bar{W}_i^{n+1} + \displaystyle\int_{t^n}^{t^{n+1}} H(W_i(t))dt = 0 \ , \end{cases} \tag{7}$$

This fractional step approach does not match the physical coupling between chemistry and fluid mechanics into the same time step, but seems to be a quite cheap method to compute stationnary and unstationnary chemically reacting flows.

In the sequel, concentrating on the second chemical step, we examine and compare various possible schemes for the integration of the chemical source terms.

2.2 One–cell model

The new system to be solved now is a system of algebraic-differential equations consisting of the κ ordinary differential equations of chemical kinetics for the mass fractions and of the conservation of energy. The unknowns are the temperature T and the vector of mass fractions Y. The system can be written as:

$$\begin{cases} \dfrac{dY_k}{dt} = \dfrac{\Omega_k(T,Y,\rho)}{\rho} = \omega_k(T,Y) \ , \\ \\ \epsilon(T,Y) = \displaystyle\sum_{k=1}^{\kappa} Y_k \epsilon_k(T) = Constant \ . \end{cases} \tag{8}$$

Notice that ρ is constant in the first equation of (8). Note also that we use the equation of conservation of energy in its integral form and not in its differential form $C_v \dfrac{dT}{dt} = -\displaystyle\sum_{k=1}^{\kappa} \omega_k \epsilon_k(T)$, with $C_v = \displaystyle\sum_{k=1}^{\kappa} Y_k C_{v\,k}$.

We now have to write in details the reactions terms appearing in (8). We consider that the composition of the mixture of κ gazeous species is influenced by I reversible chemical reactions, which we write as:

$$\sum_{k=1}^{\kappa} \nu'_{ki} \chi_k \rightleftharpoons \sum_{k=1}^{\kappa} \nu''_{ki} \chi_k \ , \tag{9}$$

for $1 \leq i \leq I$. The source terms $\omega_k = \dfrac{dY_k}{dt}$ are given by:

$$\omega_k = \sum_{i=1}^{I} W_k \nu_{ki} \mathcal{R}_i \ , \tag{10}$$

where $\nu_{ki} = (\nu''_{ki} - \nu'_{ki})$, W_k being the molar weight of species χ_k, and where $\mathcal{R}_i$ denotes the global advancement rate of the reaction i.

The reaction rate of the i-th reaction is then given by:

$$\mathcal{R}_i = K_{f,i} \prod_{k=1}^{\kappa} N_k^{\nu'_{ki}} - K_{r,i} \prod_{k=1}^{\kappa} N_k^{\nu''_{ki}} \ , \tag{11}$$

where $N_k = \dfrac{\rho Y_k}{W_k}$ is the molar density of species χ_k. For third-body reactions (see Appendix B), the expression for $\mathcal{R}_i$ is modified as:

$$\mathcal{R}_i = B_i \ (K_{f,i} \prod_{k=1}^{\kappa} N_k^{\nu'_{ki}} - K_{r,i} \prod_{k=1}^{\kappa} N_k^{\nu''_{ki}}) \ , \tag{12}$$

where $B_i = \displaystyle\sum_{k=1}^{\kappa} \alpha_{ki} N_k$; the α_{ki}'s are the third-body-efficiency coefficients of species χ_k for the reaction i.

The forward and reverse reaction rates $K_{f,i}$ and $K_{r,i}$ are given by:

$$K_{f,i} = A_i T^{\beta_i} \exp\left(-\frac{E_i}{RT}\right) \ , \quad K_{r,i} = \frac{K_{f,i}}{K_{c,i}} \ , \tag{13}$$

where E_i is the activation energy of the forward reaction, and where $K_{c,i}$ is the *equilibrium constant* for reaction i. These "constants" are given by the following expressions:

$$K_{c,i} = \left(\frac{P_{atm}}{RT}\right)^{\Delta\nu_i} \exp\left(\frac{\Delta S_i^0}{R} - \frac{\Delta H_i^0}{RT}\right) \ , \tag{14}$$

where:

$$\Delta\nu_i = \sum_{k=1}^{\kappa} \nu_{ki} \ , \quad \Delta S_i^0 = \sum_{k=1}^{\kappa} \nu_{ki} S_k^0(T) \ , \quad \Delta H_i^0 = \sum_{k=1}^{\kappa} \nu_{ki} H_k^0(T) \ , \tag{15}$$

and where P_{atm} is the value in Pascals of the atmospheric pressure: $P_{atm} = 101325$.

In (15), $S_k^0(T)$ and $H_k^0(T)$ respectively denote the standard-state molar entropies and enthalpies for species k; they are approximated using the relations:

$$\frac{S_k^0(T)}{R} = a_{1k} \ln T + a_{2k} T + \frac{a_{3k}}{2} T^2 + \frac{a_{4k}}{3} T^3 + \frac{a_{5k}}{4} T^4 + a_{7k} \ , \tag{16}$$

$$\frac{H_k^0(T)}{RT} = a_{1k} + \frac{a_{2k}}{2} T + \frac{a_{3k}}{3} T^2 + \frac{a_{4k}}{4} T^3 + \frac{a_{5k}}{5} T^4 + \frac{a_{6k}}{T} \ , \tag{17}$$

where the a_{lk} coefficients are two sets of constants given for two intervals of temperatures, the "upper" and the "lower" intervals, corresponding respectively to $T \geq T_{MID}(k)$ and $T \leq T_{MID}(k)$. We use the CHEMKIN Fortran library [6] to compute all these thermodynamic data. The CHEMKIN package also allows us to easily change the chemistry kinetic model (see Appendix B).

Lastly, the specific energy $\epsilon(T, Y) = \sum_{k=1}^{\kappa} Y_k \epsilon_k(T)$ is evaluated from the relations:

$$\epsilon_k(T) = \frac{H_k^0(T) - RT}{W_k} \ , \tag{18}$$

where the molar enthalpy $H_k^0(T)$ of species χ_k is given by (17).

3 Numerical experiments

We will now consider several numerical methods for the solution of system (8), and compare them on three typical numerical experiments.

We will see that the crucial point in all experiments, and for all methods, is the choice of the local time step. In the numerical investigation presented here, we made this choice *a priori* in a semi-empirical manner; indeed, for the complete system (6), one ideally wishes to take for the chemistry the time step coming from the stability criterion of the explicit finite-volume method for the fluid, so as to avoid evaluating the own characteristic time for the complex chemical mechanism. But we will see that many difficulties remain, and in fact that several of the methods under consideration behave very poorly for the hydrogen-air combustion test case investigated below. Nevertheless, we found it necessary to present these numerical results before we perform a detailed analysis of the numerical stability of some of the schemes for some model situations in the next section.

For some stability reasons (see [1] for the details), we slightly modify the system (8) in our experiments below: we impose the conservation of enthalpy instead of imposing the conservation of energy. In fact, this modification does not qualitatively affect the results which will be presented and discussed below.

3.1 The numerical methods

We begin by describing the methods in some details.

We will mainly consider implicit methods. The differences between the various methods considered here lie in the size of the vector of unknowns. The first method is simply Newton's method on the whole system (8), i.e. with T and Y as simultaneous unknowns. In other words, we write (8) as:

$$\left\{ \begin{array}{l} \mathcal{C}_1(X^{n+1}) = \displaystyle\sum_{k=1}^{\kappa} Y_k^{n+1} \epsilon_k(T^{n+1}) - \epsilon^0 = 0 \ , \\ \\ \mathcal{C}_{k+1}(X^{n+1}) = Y_k^{n+1} - \Delta t \ \omega_k(T^{n+1}, Y^{n+1}) + Y_k^n = 0 \ , \end{array} \right. \tag{19}$$

with:

$$X^{n+1} = \begin{pmatrix} T^{n+1} \\ Y_1^{n+1} \\ \vdots \\ Y_\kappa^{n+1} \end{pmatrix} \tag{20}$$

and $\epsilon^0 = \sum_{k=1}^{\kappa} Y_k^0 \epsilon_k(T^0)$. The Newton iterations may then be written as:

$$G^\alpha \ \Delta X^\alpha = -\mathcal{C}(X^\alpha) \ , \tag{21}$$

where $G^\alpha = \left(\frac{\partial \mathcal{C}}{\partial X}\right)^\alpha$ and $\Delta X^\alpha = X^{\alpha+1} - X^\alpha$, with $X^{\alpha=0} = X^n$ and $X^{n+1} = X^{\alpha=\alpha_{max}}$. The dimension of the unknown vector is $\kappa+1$, and the linear system is inverted at each iteration by a direct GAUSS method. The Jacobian matrix G is exactly computed at each iteration from its analytical expression (see Appendix A). In practice, we limit the number of Newton iterations to ten, in order to obtain a not too expensive method: we will call this method "coupled Newton" method (CN). If we choose $\alpha_{max} = 1$, we obtain the "coupled linearized" implicit method (CL).

We can also slightly change this approach and uncouple the mass fractions system from the energy equation in the resolution. We then only make Newton iterations on the mass fractions and solve separately for the temperature by another scalar Newton method on the energy equation. More precisely, we then write the mass fractions equations as:

$$\mathcal{U}_k(Z^{n+1}) = Y_k^{n+1} - \Delta t \ \omega_k(T^n, Y^{n+1}) + Y_k^n = 0 \ , \tag{22}$$

with:

$$Z^{n+1} = \begin{pmatrix} Y_1^{n+1} \\ \vdots \\ Y_\kappa^{n+1} \end{pmatrix} \ . \tag{23}$$

We now write the vector Newton iterations as:

$$J^\alpha \ \Delta Z^\alpha = -\mathcal{U}(Z^\alpha) \ , \tag{24}$$

with $J^\alpha = \left(\frac{\partial \mathcal{U}}{\partial Z}\right)^\alpha$, $\Delta Z^\alpha = Z^{\alpha+1} - Z^\alpha$, $Z^{\alpha=0} = Z^n$ and $Z^{n+1} = Z^{\alpha=\alpha_{max}}$, and the new temperature T^{n+1} is then computed by substituting the new mass fractions Y_k^{n+1} into the energy equation:

$$\sum_{k=1}^{\kappa} Y_k^{n+1} \epsilon_k(T^{n+1}) - \epsilon^0 = 0 \ , \tag{25}$$

and solving it by a scalar Newton method. Limiting α to $\alpha_{max} = 10$, we call this method the "uncoupled Newton" method (UN). Again, if we take $\alpha_{max} = 1$, we simply obtain a linearized implicit method, called the "uncoupled linearized" method (UL).

This uncoupled formulation allows us to also consider explicit methods. We will consider both the forward Euler method and an explicit two-stage Runge-Kutta (RK2) method, namely Gill's method (see [12] and Appendix C for more details). But these methods will be *a priori* the "worst" methods in terms of time step limitation.

Lastly, we can also use for the solution of (8) an O.D.E. solver as a (quasi) black box – and the most popular one seems to be LSODE [5] – for the mass fractions equations, with a one-variable Newton method for the temperature equation, as in the above "uncoupled" approaches. Or, in a very similar manner, we can solve the whole system with an Algebraic-Differential-Equations solver – like DASSL [9], for example.

Let us simply recall some features of the method used in LSODE. For the system of ordinary differential equations $\dot{y} = f(t, y)$, LSODE uses a backward differentiation formula :

$$y_n = \sum_{j=1}^{q} \alpha_j y_{n-j} + \Delta t^n \beta_0 f(t^n, y^n) \tag{26}$$

q is the order of accuracy of the method ($1 \leq q \leq 5$). The solution of the resulting non-linear system is computed by modified Newton iterations, where the Jacobian matrix (either exact and supplied by the user or approximated by internal difference quotients) is held constant during the iterations. The whole efficiency of the package mainly relies on the optimization of the local time step, which involves quite numerous failure tests and feedbacks. In particular, the initial time step is essentially determined by the constraint (see [5]):

$$\| \frac{h^2}{2} \ddot{y} \|_{WRMS} = 1 \ , \tag{27}$$

with the norm $\|v\|_{WRMS} = \sqrt{\frac{1}{N} \sum_{n=1}^{N} (\frac{v_i}{\epsilon_i})^2}$, the numerical tolerances ϵ_i's being supplied by the user.

Let us finally emphasize that, for all numerical experiments described below, we always use the values from the previous time step as initial guess for the Newton method.

3.2 The test-case: hydrogen-air combustion

In all numerical experiments below, we consider the combustion of a homogeneous mixture of hydrogen and air. The initial molar fractions are assumed to be:

$$X(H_2) = X(O_2) = \frac{1}{5.79} \ , \quad X(N_2) = \frac{3.79}{5.79} \ , \tag{28}$$

and zero molar fractions for all other species. The initial values of temperature and pressure are $T_i = 1615\ K$, $P_i = 0.4\ atm$. These values may be seen as typical initial values behind the shock when studying shock-induced hydrogen-air combustion, for instance in scramjets configurations. The numerical tests use two kinetic models, given in Appendix B; the first mechanism involves 9 species and 19 reactions, the second one involves 10 species and 16 reactions. The final equilibrium temperature is equal to 2637 K for both models. We assume that the mixture combustion has reached its equilibrium before time $t_{max} = 10^{-4}\ s$, which has been taken as the final time of our calculations.

We should keep in mind in the sequel that we have chosen here a quite severe test-case. It will indeed appear that most numerical methods behave much better for globally endothermic chemical mechanisms (such as the kinetic model describing the air chemistry) than for exothermic chemistries; moreover, among the exothermic mechanisms, the combustion of hydrogen is more explosive and exothermic than the combustion of heavier hydrocarbons.

3.3 First numerical experiment

As a first numerical experiment, we solve the above test-case with all methods presented in Section 3.1, using the following simple strategy for choosing the variable time step.

As already said, the time step cannot be chosen in an arbitrary way, since some of the methods suffer from severe stability condition (see Section 4). Here, we choose to reduce the time step during the calculation, i.e. while the temperature increases, in the following simple and crude way. For all methods (except for LSODE and DASSL which evaluate their own time steps), we take the initial time step to be $\Delta t_0 = 10^{-9}\ s$. Then, for several values θ_l of the temperature, we simply multiply the initial time step Δt_0 by some factor ϵ_l when the temperature T is exceeding the value θ_l. The values of θ_l and ϵ_l are chosen to be *a priori* the same for all methods (after having tried quite a number of values...) and are equal to:

θ_1	θ_2	θ_3	θ_4	θ_5	θ_6	θ_7	θ_8
1650	1700	1800	1900	1950	2000	2100	2200
ϵ_{θ_1}	ϵ_{θ_2}	ϵ_{θ_3}	ϵ_{θ_4}	ϵ_{θ_5}	ϵ_{θ_6}	ϵ_{θ_7}	ϵ_{θ_8}
0.2	0.1	0.05	0.02	0.01	0.005	0.001	0.0005

Moreover, these empirical values can be changed during the numerical calculation: whenever the code crashes, the current value of ϵ_l is then divided by two and the calculation proceeds.

The numerical results obtained in this way are very similar for all methods (the plotted profiles are undistinguishable) and accurate. The time evolution of the temperature for both 9-19 and 10-16 chemistry models, presented on Figure 1, shows that the equilibrium temperature is reached slightly earlier with the 10-16 mechanism than with the 9-19 model. The mass fractions profiles are shown on Figure 2 for the 9-19 model, and on Figure 3 for the 10-16 mechanism (for the latter, we have omitted the H_2 and O_2 profiles, which look very much like those on Figure 2, but for the shorter equilibrium time). Notice that, for the 10-16 model, the species N_2 and NO have not reached equilibrium at the final time 10^{-4} s.

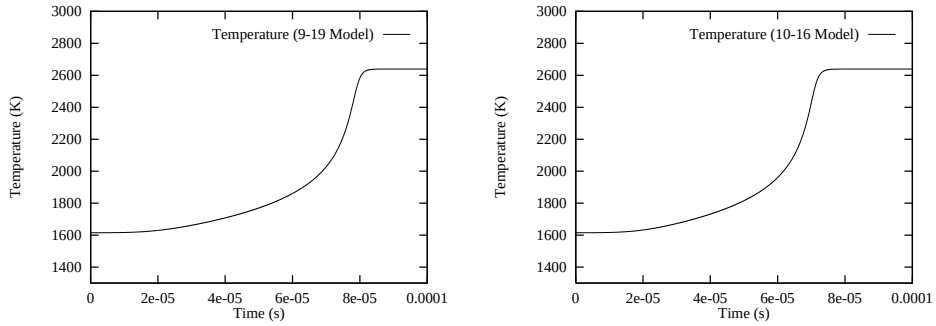

Figure 1: Temperature evolution for both 9-19 and 10-16 models.

But the most important output of this experiment concerns the comparison of the numbers of time steps and of the CPU times needed by each of the methods. These figures are given in the Table below, and are particularly dramatic (the calculations were performed on an IBM RS-6000 560 computer) !!

Methods	CPU time	Number of iterations
RK2	17 h	2.6 10^8
UL	1 h 30 mn	2.6 10^6
CL	11 h 30 mn	3 10^7
UN	50 h (!)	8 10^7
CN	$>$ 100 h (!!!)	$>$ 1 10^8
LSODE	0.5 s	144
DASSL	0.7 s	121

These results deserve several comments. First, they show undoubtedly that only the specialized O.D.E. and D.A.E. solvers LSODE and DASSL can be used efficiently for such a complex and stiff chemistry problem. Notice however that the above results do not bring any definite conclusion for the comparison of LSODE and DASSL for this problem: the performances of both methods are very close; moreover, when we also tried LSODE and DASSL methods on a SUN SS10 computer, their respective CPU times were 1.08 s for LSODE and 0.86 s for DASSL: the relative performances of LSODE and DASSL are therefore machine-dependent.

Besides, all other methods behave very poorly. We may also say that the linearized implicit methods seem (in each case, either coupled or uncoupled) to be less unstable than the Newton method, and also that uncoupled methods seem to give better results than coupled ones. But the main conclusion is certainly that all these methods need a considerable CPU time!

Before turning to our second numerical experiment, we should emphasize again two facts. On one hand, the above results are very far from being optimal, because we used a very poor strategy for

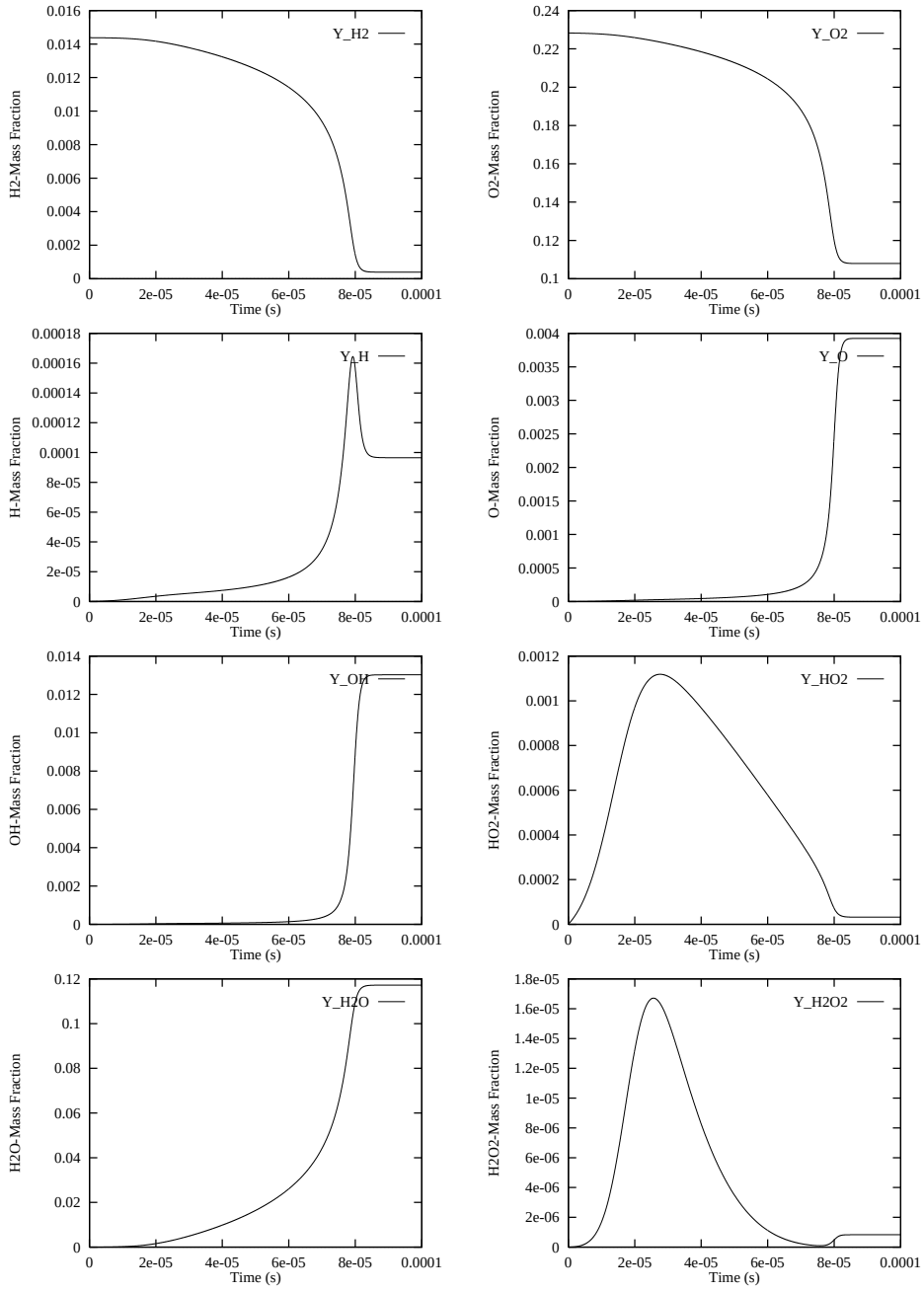

Figure 2: Mass fractions evolution for the 9-19 model.

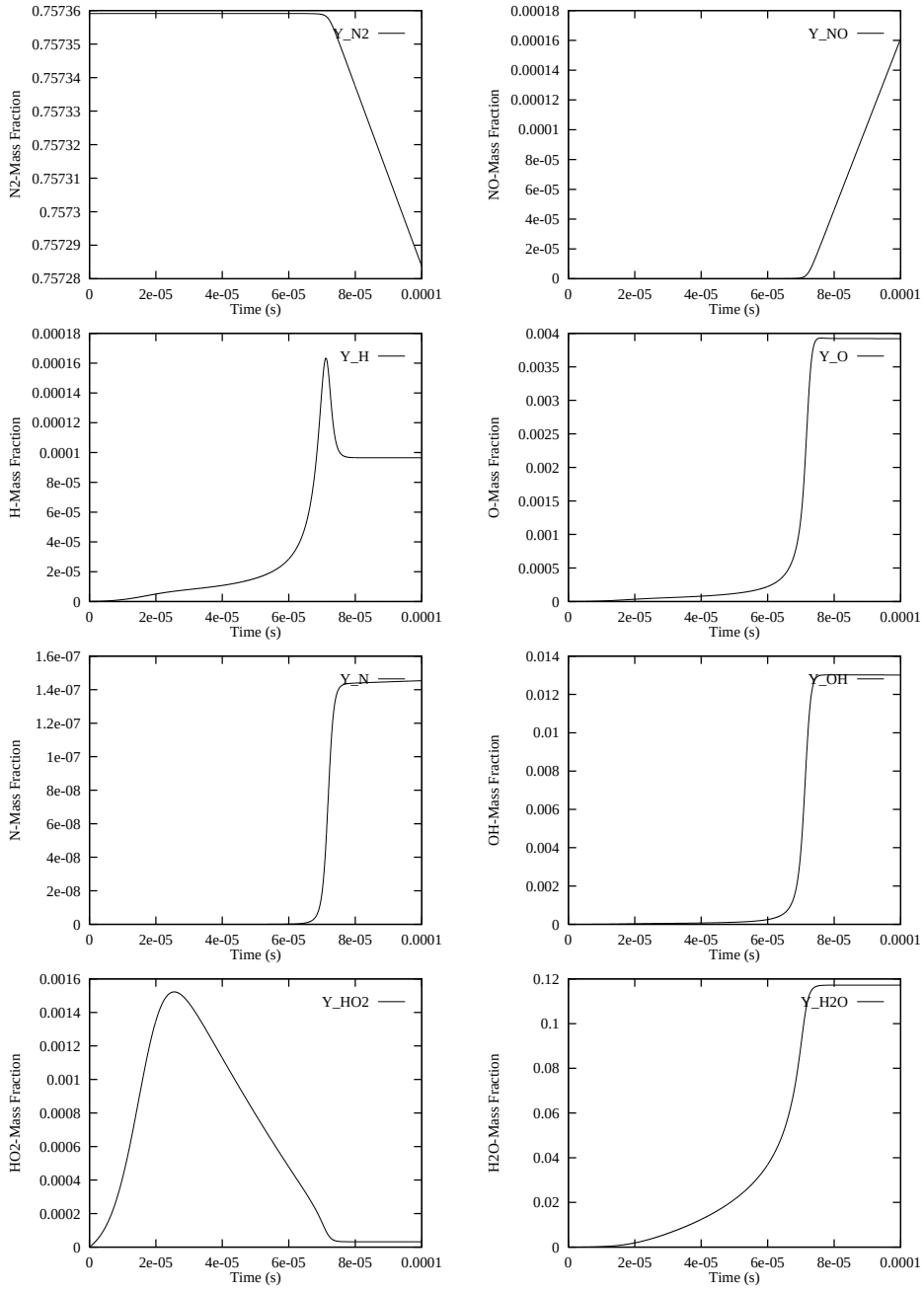

Figure 3: Mass fraction evolution for the 10-16 model.

adjusting the local time step; much better results will indeed be obtained in our third experiment below. On the other hand, it is worth to keep in mind that our sole criterion for diminishing the time step in this experiment was the crash of the code. We could have decided to decrease Δt whenever one of the mass fraction(s) was becoming negative (this actually happened during the calculation, but very slightly ($\sim 10^{-7}$ in absolute value for the greater ones); the code crashed when more negative values were appearing). We will see in the next experiments that forcing the mass fractions to remain non negative would have led to quite different results.

3.4 Second numerical experiment

We now investigate more closely the size of the time step with which each of the methods can adequately operate. In our second experiment, we are going to determine, for each method except LSODE and DASSL (but adding the forward Euler explicit method), and for both 9-19 and 10-16 kinetic models, the maximal time step required so as to ensure that all mass fractions stay in the interval $[0, 1]$. This will be done for an initial pressure equal to the atmospheric pressure, and for an initial temperature increasing from 1300 K to 2300 K with a step of 20 K.

We will consider two different initial compositions. First, we take the same initial composition as in the above section, i.e. with zero mass fractions for species other than H_2, O_2 and N_2. We will call this initial condition "zero composition" and the maximal allowed time step will be denoted $\Delta t^+_{Y=0}$. Secondly, we leaded the same calculation by initiating the mass fractions with the values calculated by LSODE at the time $t = 10^{-6}\tau$, where τ is the ignition delay at the considered temperature; this initial condition will be called "non-zero composition", and the corresponding maximal time step is denoted $\Delta t^+_{Y>0}$. Let us make precise that we call here "ignition delay" the time where the temperature profile changes its curvature (i.e. the inflexion point), starting from the zero-composition mixture; this is a characteristic time for the combustion of this mixture at a given temperature (see Figure 4).

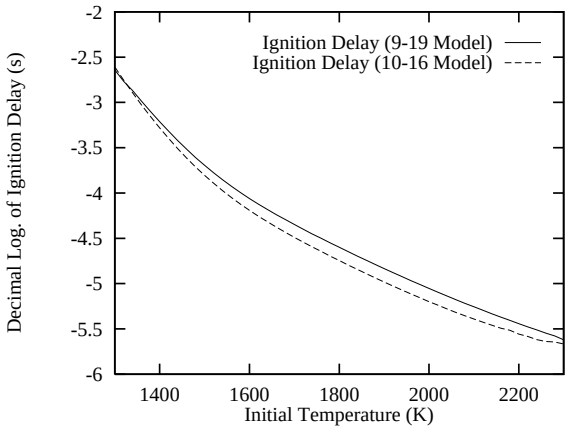

Figure 4: Ignition delay as a function of the initial temperature.

The results are presented on Figures 5 to 10.

These results show for instance that using the "non-zero" initial mass fractions does not necessarily increase the maximal usable time step, as we could expect: we sometimes have $\Delta t^+_{Y=0} > \Delta t^+_{Y>0}$ (and even $\Delta t^+_{Y=0} \gg \Delta t^+_{Y>0}$ for the UN method).

But the most interesting result is that the initial time step $\Delta t^+_{Y=0}$ actually vanishes to zero (with machine accuracy) at some intial temperatures for some of the implicit methods(CL, UL and CN, for both chemistry models). In other words, for this (not so particular !) initial condition, these methods *can never lead to non-negative mass fractions* for this hydrogen-air combustion process. Moreover, the improvement brought by using the "non-zero composition" is absolutely not sufficient in several cases, since $\Delta t^+_{Y>0}$ is highly oscillating with the temperature; this is true for the CL and CN methods on the 10-16 model. For most methods, the 9-19 mechanism gives worse results than the 10-16 model for the "zero composition", but the advantage from using the "non-zero" initial mass fractions seems bigger.

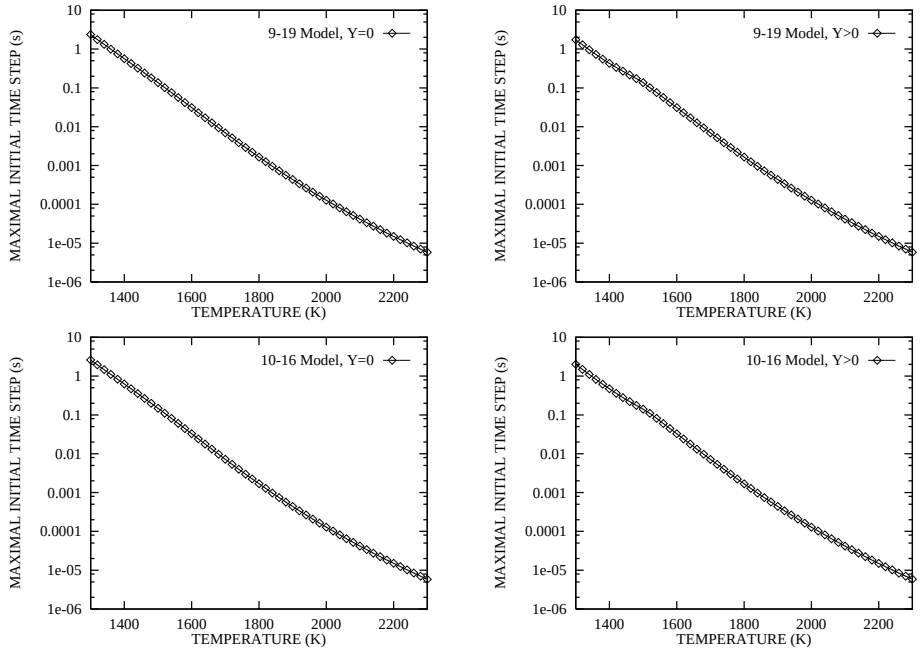

Figure 5: Maximal time steps for the first-order explicit method.

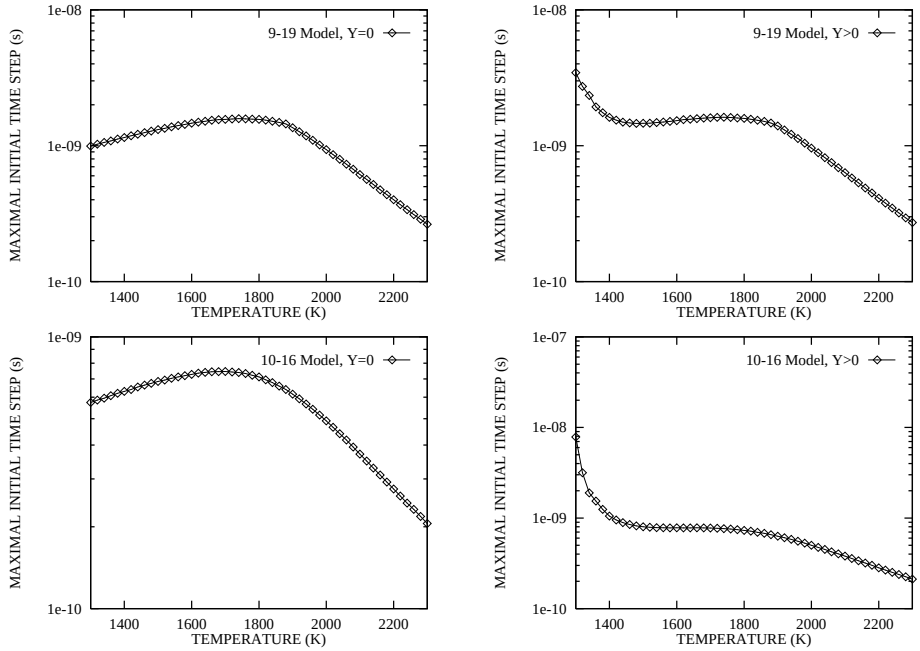

Figure 6: Maximal time steps for the RK2 method.

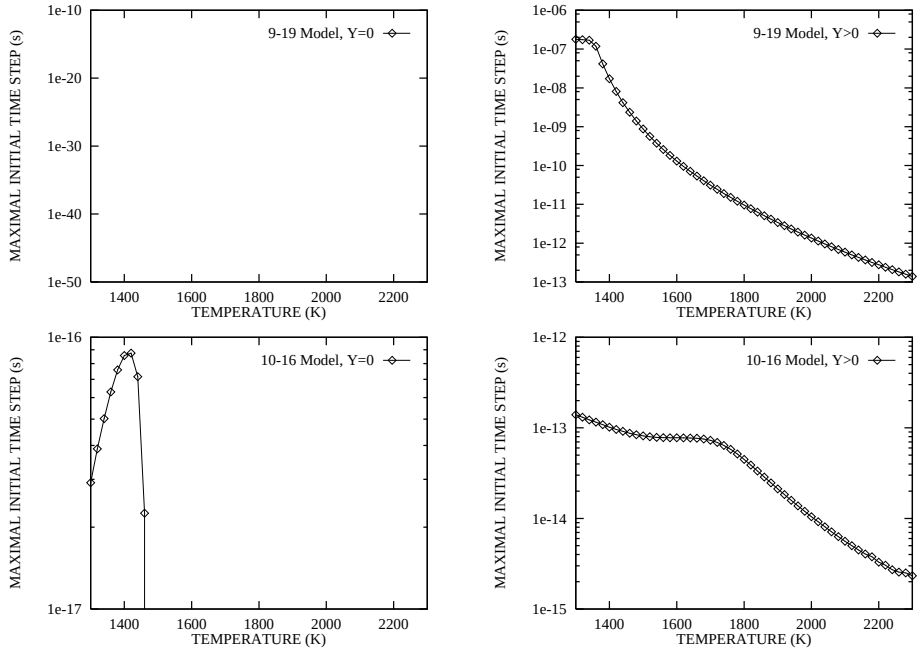

Figure 7: Maximal time steps for the UL method.

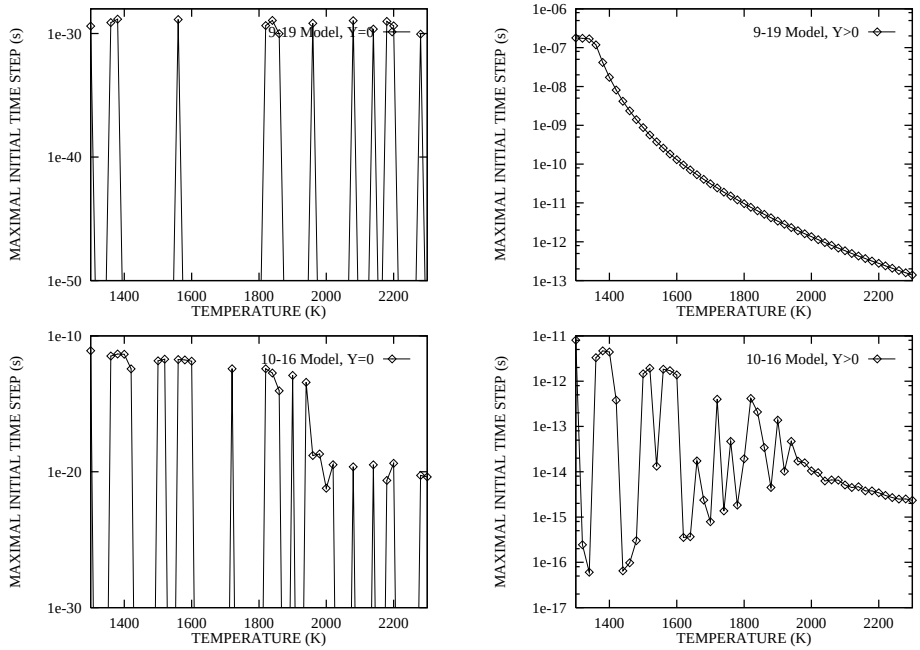

Figure 8: Maximal time steps for the CL method.

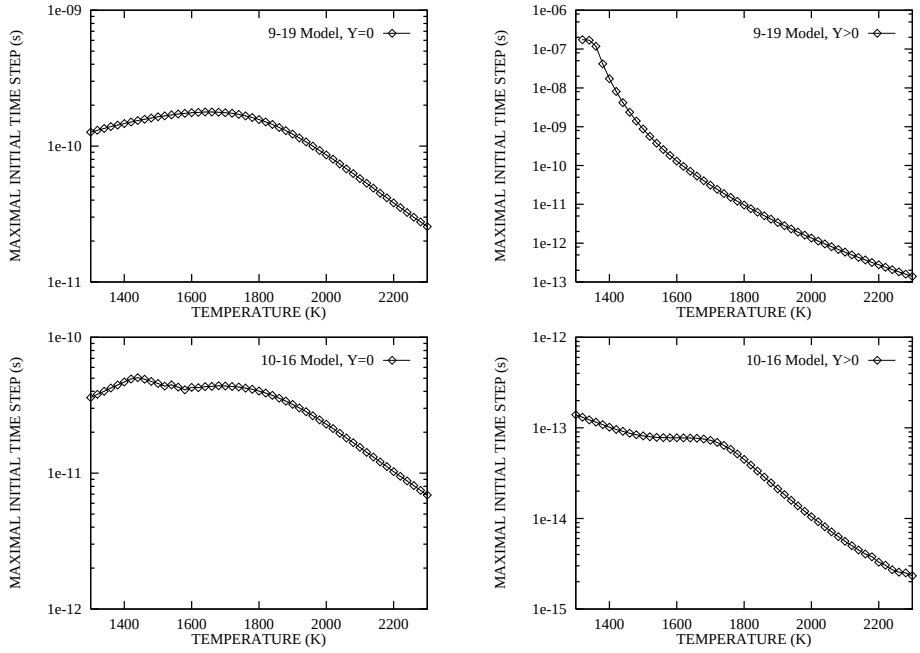

Figure 9: Maximal time steps for the UN method.

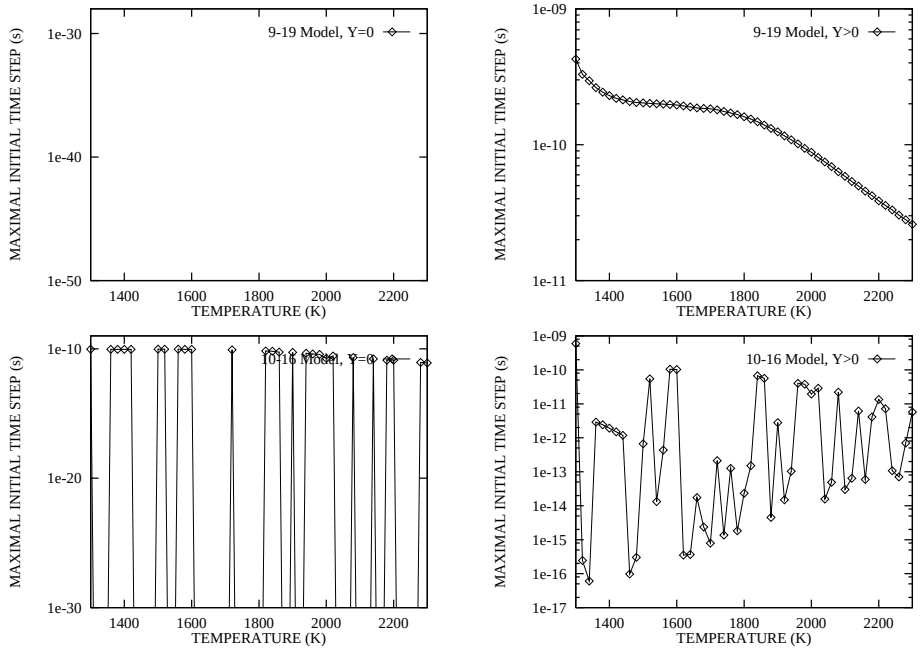

Figure 10: Maximal time steps for the CN method.

Another paradoxical result lies in the fact that the first-order explicit and explicit RK2 methods have the larger allowed time step !! In fact, this is not too surprising since our choice of the time step only demands that mass fractions stay between 0 and 1, but does not necessarily give physically reasonable results (see our third experiment below).

Also, we need to add that, if instead of imposing non-negative mass fractions, we were requiring mass fractions "not too far" from the interval $[0, 1]$ (and above all that the code does not crash, as in our first experiment), the linearized implicit methods would appear to allow larger time steps than the explicit or Newton methods. In all cases, we must admit that the Newton methods again behave surprinsingly poorly.

3.5 Third numerical experiment

For our last experiment, we again consider the test-case of Section 3.2. But we will use a more elaborate stategy for choosing the variable time step, while imposing the mass fractions to stay between 0 and 1. We carried out these calculations only for the 9-19 model (which seems harder than the 10-16 one, at least at the beginning of the computation, from the previous section).

Our (empirical) time step strategy goes as follows: starting with a given value of Δt, we constantly check whether the mass fractions remain in the admissible interval. In case of failure, we multiply Δt by a coefficient $\alpha < 1$. But we may also increase the time step using some fixed integers N_l and coefficients $\beta_l > 1$, as follows: if the computation remains successful during N_l iterations, we then multiply Δt by β_l. Also, after $M > \max N_l$ successful iterations, we multiply Δt *at each time step* by a coefficient $\gamma > 1$.

For the first-order explicit and second-order explicit RK2 methods, the initial values of Δt, the values of N_l, α, β_l, M and γ are given in the Table below, together with the total number of iterations and the CPU time in seconds on an IBM RS-6000 560 computer (we always took $\beta_2 = \beta_3 = \beta_4$).

Methods	Initial Δt	α	N_1	β_1	N_2	N_3	N_4	β_2	M	$\gamma - 1$	Iter.	CPU
EXPL	$1.2\ 10^{-9}$	0.9	15	1.002	100	500	1000	1.005	2000	5.10^{-5}	790 000	260
RK2	$1.4\ 10^{-9}$	0.9	15	1.02	100	500	1000	1.05	2000	0.01	835 000	1093
UN	$1.0\ 10^{-11}$	0.9	15	1.002	100	500	1000	1.005	2000	5.10^{-5}	2079 000	47323

In agreement with the previous section, the same experiment cannot directly be run with the UL, CL and CN methods, since $\Delta t^+_{Y=0}$ vanishes for these methods. Instead, we started with the "non-zero composition", i.e. with the mass fractions obtained by LSODE at a time of $7.852\ 10^{-11}$ seconds, corresponding to 10^{-6} times the ignition time of the reaction at $T = 1615\ K$. The parameters and results of the calculation are given below:

Methods	Initial Δt	α	N_1	β_1	N_2	N_3	N_4	β_2	M	$\gamma - 1$	Iter.	CPU
UL	$1.0\ 10^{-10}$	0.9	15	1.002	100	500	1000	1.005	2000	5.10^{-5}	753 000	3543
CL	$1.0\ 10^{-10}$	0.9	15	1.002	100	500	1000	1.005	2000	5.10^{-5}	738 000	7422
CN	$1.0\ 10^{-10}$	0.9	15	1.002	100	500	1000	1.005	2000	5.10^{-5}	Failure	

For the CN method, the calculation fails after 15500 iterations. The time step size required to conserve non-negative mass fractions first lies between 5.10^{-10} and 7.10^{-9} seconds, but then vanishes after time $t = 7.10^{-6}\ s$. It seems hard to choose the initial composition so that the mass fractions never become negative.

The results of these calculations are shown on Figures 11 to 15. For each method, we show the evolution of the time step, and those profiles (of temperature and mass fractions) where some particularities can be remarked. Indeed, in most cases, the temperature and mass fractions profiles perfectly agree with those of the first experiment, i.e. are perfectly acceptable.

The first comment is that these results have been obtained with much shorter computational times than in our first experiment, i.e. we have used bigger time steps on the average, while preserving the mass fractions positivity. The first-order explicit method performs surprisingly well; the linearized implicit methods, which need a little help (with the "non-zero" initialisation) to start the calculation,

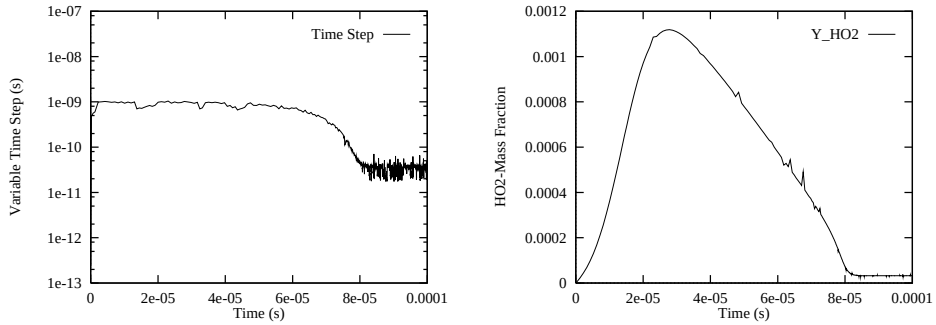

Figure 11: Variable time step and HO_2 mass fraction for the first-order explicit method.

perform equally well in terms of time step size (and therefore wose in terms of CPU time). And again, the Newton methods perform very badly.

However, the results present in general some oscillations for the mass fractions, in particular for the rare species; therefore, requiring the mass fractions to remain non-negative does not insure accurate non oscillatory results. In particular, the results of the RK2 method are fully unacceptable ! But a careful examination also shows that the results of the UN method (which are the most oscillatory among all other methods) are also false: we see indeed that the equilibrium temperature is reached much earlier than in the first experiment (this wrong result is probably due to the oscillations which are produced before the equilibrium on the mass fractions profiles).

It is also worth noticing a rather surprising fact: all methods see their variable time step decrease during the calculation, and highly oscillate when they reach equilibrium. As a consequence, most of the computational time is employed to go from equilibrium to the final time. with a time step which is more than ten times smaller than the average time step used before equilibrium!

4 Numerical analysis of some simple models

The results of the numerical experiments presented above are surprising in several aspects, and require some explanation. This is the objective of this section, where we analyze several simpler models (the full hydrogen-air mechanism being out of reach for an analytical investigation).

Our numerical analyses will indeed explain several of the results observed above. In particular, we will examine on several examples the stability limits of the coupled and uncoupled linearized implicit methods; we will see why these methods behave much better for globally endothermic chemical mechanisms than for exothermic chemistries, and that, in the latter case, they may suffer from stability restrictions which are even more severe than the stability limit of the first-order explicit method !!

In the analyses below, we will say that a numerical method is stable (for a given time step) if it preserves the inequalities $0 \leq Y_k \leq 1$ for all species (in such a case, lower and upper bounds for the temperature follow from the energy conservation).

4.1 The simple reversible model

4.1.1 Describing the model

We begin by considering the simple reversible reaction:

$$A \rightleftharpoons B \ . \tag{29}$$

For the sake of simplicity, we will assume here that both species A and B have constant and equal specific heats at constant pressure: $C_{vA} = C_{vB} = C_v$; they also have the same molar weight $W_A = W_B = W$. Using the notations of Section 2.2, we will assume that $Q = H_A^0 - H_B^0 = \epsilon_A^0 - \epsilon_B^0 > 0$, which means that the forward reaction $A \longrightarrow B$ is exothermic. Lastly, let Y and Z denote the mass fractions

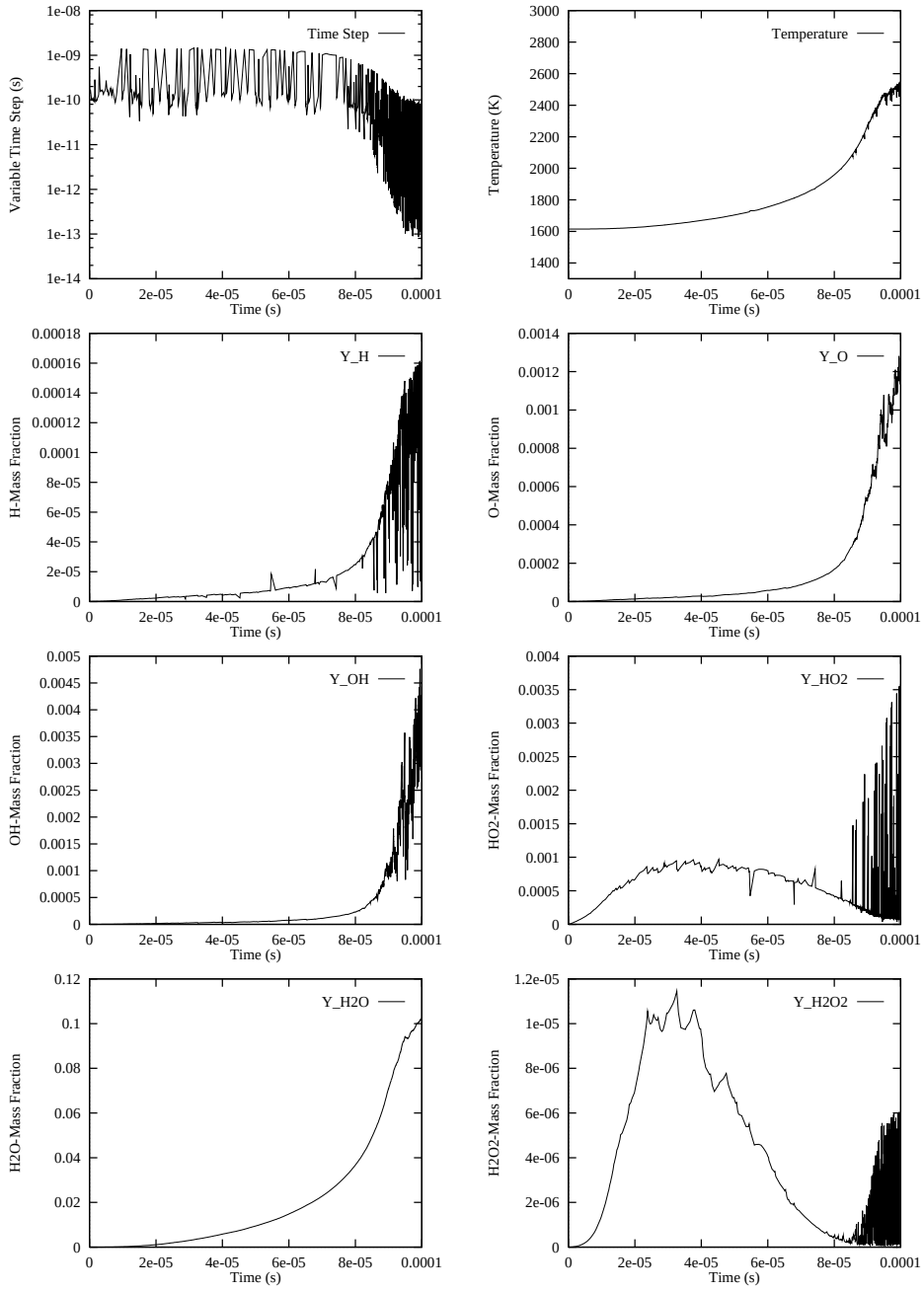

Figure 12: Variable time step, temperature and mass fractions profiles for the RK2 method.

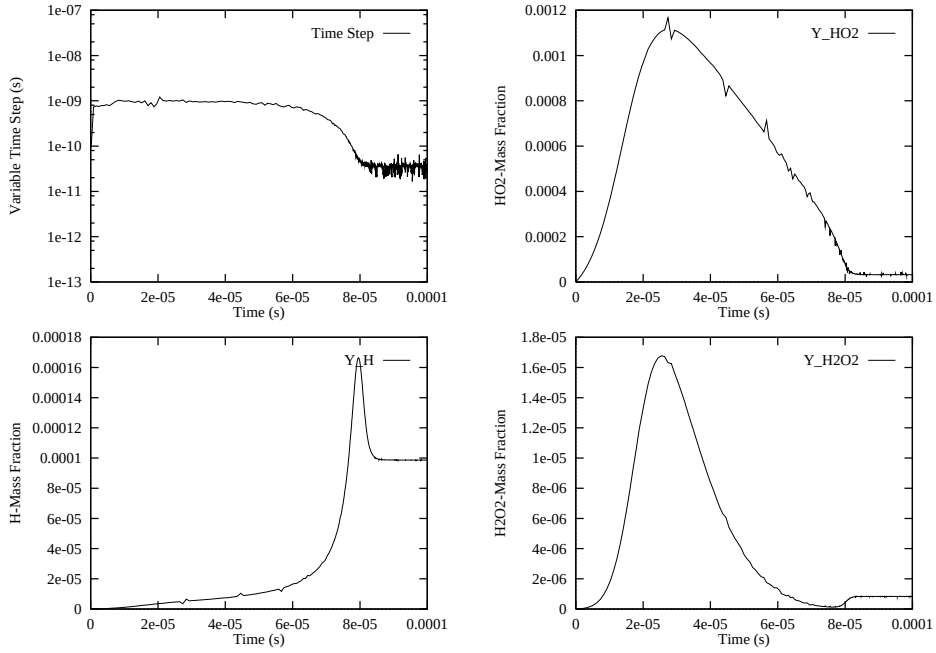

Figure 13: Variable time step and mass fractions profiles for the UL method.

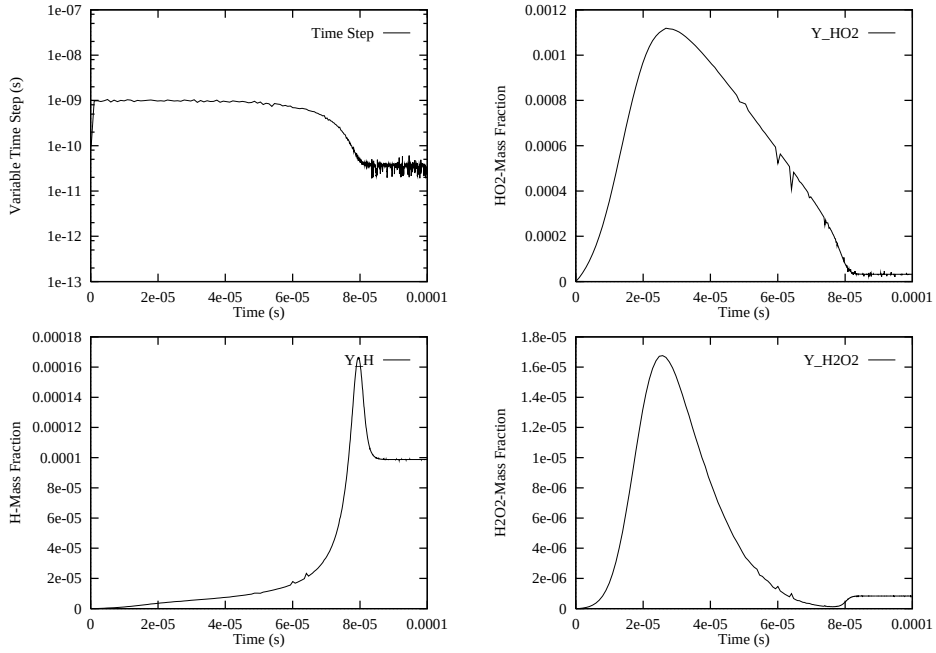

Figure 14: Variable time step and mass fractions profiles for the CL method.

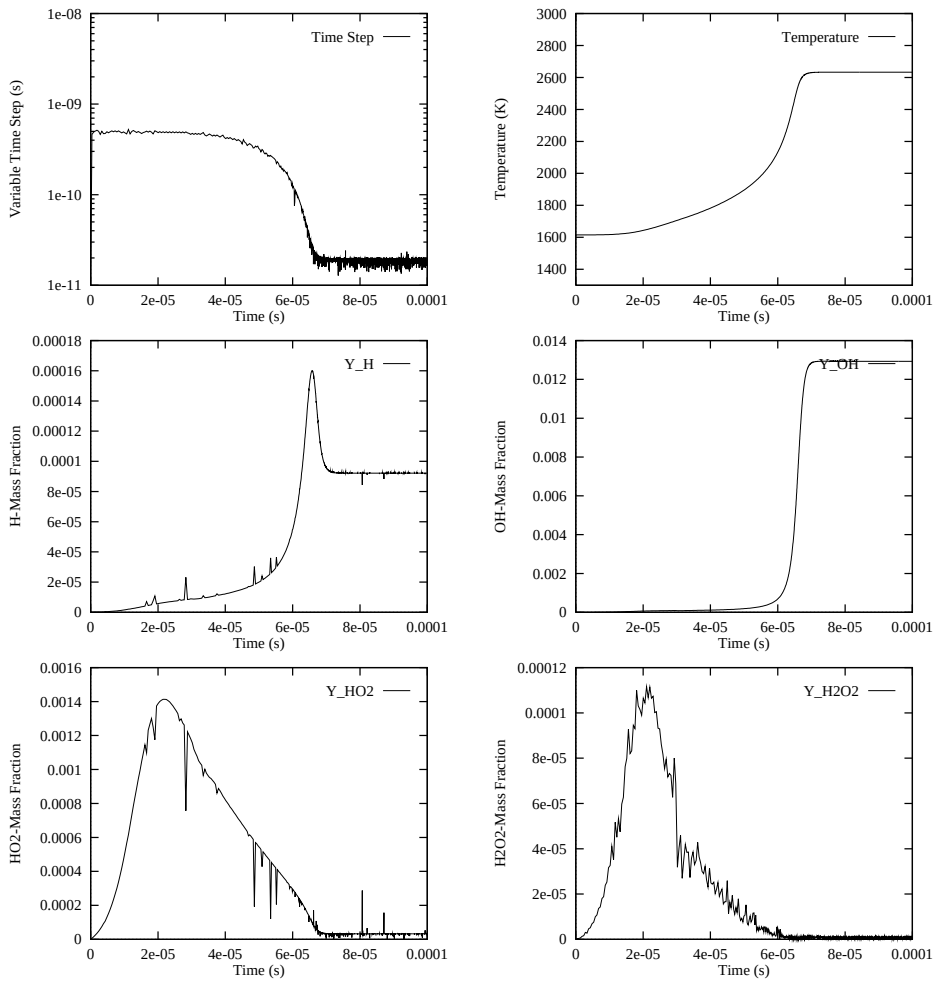

Figure 15: Variable time step, temperature and mass fractions profiles for the UN method.

of A and B respectively. System (8) now takes the form:

$$\left\{ \begin{array}{l} \dfrac{dY}{dt} = -\dfrac{W}{\rho} Y k_1(T) + \dfrac{W}{\rho} Z k_2(T) \stackrel{def}{=} -Y f_1(T) + Z f_2(T) \ , \\ \\ \dfrac{dZ}{dt} = Y f_1(T) - Z f_2(T) \ , \\ \\ \epsilon(T,Y,Z) = Y(\epsilon_A^0 + WC_vT) + Z(\epsilon_B^0 + WC_vT) = Constant \ , \end{array} \right. \tag{30}$$

with:

$$f_1(T) = A_1 T^\beta \exp\left(-\frac{E_1}{RT}\right) \ , \quad f_2(T) = A_2 T^\beta \exp\left(-\frac{E_2}{RT}\right) \ ; \tag{31}$$

the fact that the two reaction rates f_1 and f_2 involve the same exponent β, as well as the relation:

$$E_2 = E_1 + Q \ , \tag{32}$$

follow from the relations (13), (14) and (15).

We recall that C_v and ρ are constant in system (30), and we set $U = \dfrac{Q}{WC_v}$. Obviously, any solution of this system satisfies the identities:

$$Y + Z = 1 \ , \quad T + UY = Constant \stackrel{def}{=} H^0 \ . \tag{33}$$

Since all numerical methods considered below also preserve these relations, we may simply rewrite the system (30) as:

$$\left\{ \begin{array}{l} \dfrac{dY}{dt} = -Y f_1(T) + (1-Y) f_2(T) \ , \\ \\ T + UY = H^0 \ . \end{array} \right. \tag{34}$$

This system is completed with initial conditions: $Y = Y^0$, $T = T^0$.

Remark 4.1: Below, we will sometimes need to consider realistic values for the constants and variables of the problem. These values are obtained form the the following estimates and relations: we have $Y \in [0,1]$, $T \in [T_{min}, T_{max}]$, with $T_{max} = H^0$, $(T_{max} - T_{min}) = U$; typically, we have $\dfrac{T_{max}}{T_{min}} \approx 5$ to 8 and $\dfrac{E_1}{RT_{max}} \approx 4$ to 10. Also, from Mayer's relation, $(\gamma - 1)WC_v = R$, where γ is the specific heat ratio $\dfrac{C_p}{C_v}$. •

Now, the differential form of the temperature equation, consistent with (34), writes:

$$\frac{dT}{dt} = UY f_1(T) - U(1-Y) f_2(T) \ . \tag{35}$$

In view of these relations, the region:

$$\mathcal{R}_- = \{(Y,T), \ Y f_1(T) - (1-Y) f_2(T) < 0\} \tag{36}$$

of the (Y,T) plane will be called the *endothermic domain*, whereas the region:

$$\mathcal{R}_+ = \{(Y,T), \ Y f_1(T) - (1-Y) f_2(T) > 0\} \tag{37}$$

will be called the *exothermic domain*. Both domains are separated by the *equilibrium curve*, defined as:

$$Y = \frac{f_2(T)}{f_1(T) + f_2(T)} \stackrel{def}{=} Y^{\rm eq}(T) \tag{38}$$

(notice that $Y^{eq}(T) \in (0,1)$ for any temperature T). Using (31) and (32), it is easy to see that $Y^{eq}(T)$ is a monotone increasing function of T; furthermore, the asymptotic solution of system (34) as t tends to $+\infty$, which we denote as (Y^∞, T^∞), is uniquely determined by the system:

$$Y^\infty = Y^{eq}(T^\infty) \ , \quad T^\infty + UY^\infty = H^0 \tag{39}$$

(see Figure 16).

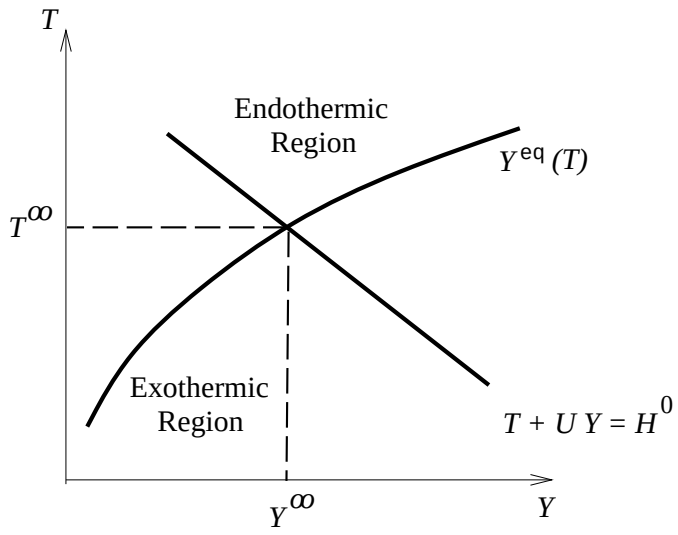

Figure 16: The equilibrium curve.

We are going to carry out the numerical analysis of system (34) with the assumption that the activation energies are high enough. More precisely, we will assume that:

$$\frac{E_2}{RT_{max}} \geq 2 \ , \tag{40}$$

and also that:

$$\beta \geq 0 \ . \tag{41}$$

4.1.2 Numerical analysis

We can now analyse how several of the numerical methods considered in Section 3 behave when applied to the simple reversible model (29).

We begin with the following simple result for the UN and UL methods:

Proposition 4.2:
For the simple reversible reaction (29)*, the uncoupled Newton and uncoupled linearized methods are unconditionnally stable.* •

PROOF: Since system (34) is linear with respect to the mass fraction Y, the UN and UL methods coincide in the present case. They take the form:

$$\begin{cases} \dfrac{Y^{n+1} - Y^n}{\Delta t} = \left(-Y^{n+1} f_1(T^n) + (1 - Y^{n+1}) f_2(T^n)\right) \ , \\ \\ T^{n+1} + UY^{n+1} = H^0 \ . \end{cases} \tag{42}$$

Then, we get:

$$Y^{n+1} = \frac{\dfrac{Y^n}{\Delta t} + f_2(T^n)}{\dfrac{1}{\Delta t} + (f_1(T^n) + f_2(T^n))} \ , \tag{43}$$

and we easily see that Y^{n+1} lies between 0 and 1 as soon as Y^n does. •

The situation is more complex for the CL method. We will prove the following:

Proposition 4.3:
For the simple reversible reaction (29)*, the coupled linearized method is not unconditionnally stable.*
However, if the assumptions (40) *and* (41) *hold, then the coupled linearized method is unconditionally stable in the endothermic domain* $\mathcal{R}_-$. •

More precise statements will be made below about the actual stability restrictions in the cases where unconditional stability does not hold, i.e. in some parts of the exothermic domain.
The proof of Proposition 4.3 consists of three Lemmas:

Lemma 4.4:
Let (Y^n, T^n) *be the discrete temperature and mass fraction computed with the coupled linearized method.*
There exists a $\mathcal{C}^1$ *monotone increasing curve* $Y = Y^*(T)$*, with:*

$$Y^{\rm eq}(T) < Y^*(T) < 1 \ , \tag{44}$$

such that $0 \leq Y^{n+1} \leq 1$ *for any* $\Delta t > 0$ *as soon as* $0 \leq Y^n \leq Y^*(T^n)$. •

PROOF: The CL scheme takes the form:

$$\left\{ \begin{array}{rl} \dfrac{Y^{n+1} - Y^n}{\Delta t} = & \big(-Y^{n+1} f_1(T^n) + (1 - Y^{n+1}) f_2(T^n) \\ & -Y^n f_1'(T^n)(T^{n+1} - T^n) + (1 - Y^n) f_2'(T^n)(T^{n+1} - T^n)\big) \ , \\ & \\ T^{n+1} + U Y^{n+1} = H^0 \ , & \end{array} \right. \tag{45}$$

from which we get:

$$Y^{n+1} = \frac{\dfrac{Y^n}{\Delta t} + f_2(T^n) + U Y^n \left(-Y^n f_1'(T^n) + (1 - Y^n) f_2'(T^n)\right)}{\dfrac{1}{\Delta t} + (f_1(T^n) + f_2(T^n)) + U \left(-Y^n f_1'(T^n) + (1 - Y^n) f_2'(T^n)\right)} \ . \tag{46}$$

Assume now that $Y^n \in [0, 1]$. If the term $-Y^n f_1'(T^n) + (1 - Y^n) f_2'(T^n)$ is non-negative, it is then clear that $0 \leq Y^{n+1} \leq 1$ for any $\Delta t > 0$. This condition writes:

$$Y^n \leq \frac{f_2'(T^n)}{f_1'(T^n) + f_2'(T^n)} \stackrel{def}{=} Y^*(T^n) \ . \tag{47}$$

From the form (31) of f_1 and f_2, we get:

$$f_i'(T) = \left(\beta + \frac{E_i}{RT}\right) \frac{f_i(T)}{T} \ , \tag{48}$$

for $i = 1, 2$. From (32), this shows that, for any T:

$$\frac{f_1'(T)}{f_2'(T)} > \frac{f_1(T)}{f_2(T)} \ , \tag{49}$$

whence $Y^*(T) > Y^{eq}(T)$ from (38) and (47). •

Now, the endothermic domain $\mathcal{R}_-$ is a subset of the region $\{(Y,T)\ ,\ \ 0 \le Y \le Y^*(T)\}$ from (44), as shown on Figure 17.

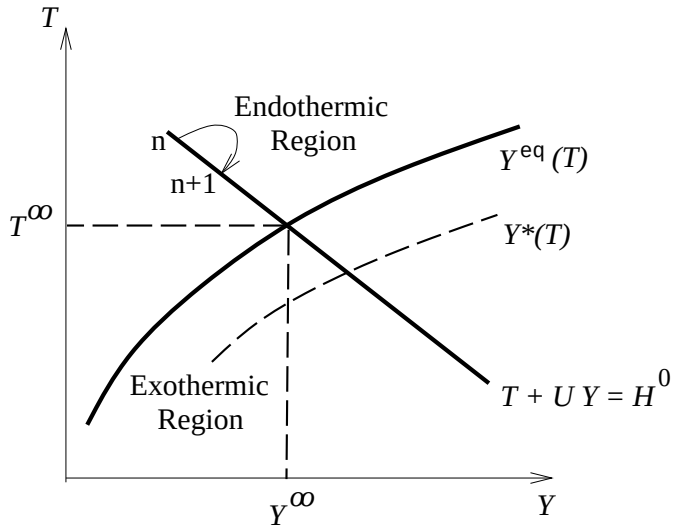

Figure 17: The equilibrium curve and the curve $Y = Y^*(T)$.

Therefore, in order to show that the CL method is unconditionally stable in the endothermic region, it remains to prove the following:

Lemma 4.5:
Let (Y^n, T^n) be the discrete temperature and mass fraction computed with the coupled linearized method.
Assume that the technical assumptions (40) *and* (41) *hold, and that* $(Y^n, T^n) \in \mathcal{R}_-$. *Then,* $(Y^{n+1}, T^{n+1}) \in \mathcal{R}_-$. •

PROOF: Assume that $(Y^n, T^n) \in \mathcal{R}_-$. We rewrite (46) as:

$$Y^{n+1} = Y^n + \frac{(-Y^n f_1(T^n) + (1-Y^n) f_2(T^n))}{\frac{1}{\Delta t} + (f_1(T^n) + f_2(T^n)) + U\,(-Y^n f_1'(T^n) + (1-Y^n) f_2'(T^n))}\ . \tag{50}$$

The right-hand side of (50) is a bounded monotone increasing function of the time step, which we will denote as $Y^{n+1}(\Delta t)$. Therefore, for any $\Delta t > 0$, we have:

$$Y^{n+1}(\Delta t) < \lim_{\Delta t \nearrow +\infty} Y^{n+1}(\Delta t) \stackrel{def}{=} \hat{Y}^{n+1}\ . \tag{51}$$

But, introducing the function $g(Y)$ defined as:

$$g(Y) = -Y f_1\left(H^0 - UY\right) + (1-Y) f_2\left(H^0 - UY\right)\ , \tag{52}$$

it is easy to check that $\hat{Y}^{n+1}$ satisfies:

$$g(Y^n) + \frac{dg}{dY}(Y^n)(\hat{Y}^{n+1} - Y^n) = 0\ . \tag{53}$$

Since g is non-negative and satisfies $g(Y^\infty) = 0$, the proof of Lemma 4.5 will be complete if we show that g is convex in the endothermic region, i.e. for $Y < Y^\infty$; we will then have $Y^n < \hat{Y}^{n+1} < Y^\infty$, whence $(Y^{n+1}, T^{n+1}) \in \mathcal{R}_-$ for any Δt (see Figure 17).

Let us therefore prove that g is convex in the endothermic region. For the sake of simplicity, we denote $T^H(Y) = H^0 - UY$. The first derivative of g is given by:

$$g'(Y) = -f_1\left(T^H(Y)\right) - f_2\left(T^H(Y)\right) - U\left[-Yf_1'\left(T^H(Y)\right) + (1-Y)f_2'\left(T^H(Y)\right)\right] \ . \tag{54}$$

In the endothermic region, we have $Y < Y^*\left(T^H(Y)\right)$ from (44) and the monotonicity of Y^* (see Figure 17), which shows that the term between brackets in (54) is positive. Therefore, $g'(Y) < 0$ for $Y < Y^\infty$.

A second differentiation yields, after some algebra:

$$\begin{aligned} g''(Y) = \quad & 2U\left(f_1'\left(T^H(Y)\right) + f_2'\left(T^H(Y)\right)\right) \\ & + \left(\frac{U}{T^H(Y)}\right)^2 \left[-Yf_1\left(T^H(Y)\right)\left(\chi_1^2 - \chi_1 - \frac{E_1}{RT^H(Y)}\right)\right. \\ & \left. + (1-Y)f_2\left(T^H(Y)\right)\left(\chi_2^2 - \chi_2 - \frac{E_2}{RT^H(Y)}\right)\right] , \end{aligned} \tag{55}$$

with $\chi_i = \beta + \dfrac{E_i}{RT^H(Y)}$ for $i = 1, 2$. Using (32), we can rewrite this as:

$$\begin{aligned} g''(Y) = \quad & 2U\left(f_1'\left(T^H(Y)\right) + f_2'\left(T^H(Y)\right)\right) + \left(\frac{U}{T^H(Y)}\right)^2 \left(\frac{Q\chi Y f_1\left(T^H(Y)\right)}{RT^H(Y)}\right) \\ & + \left(\frac{U}{T^H(Y)}\right)^2 \left[\left(\chi_2^2 - \chi_2 - \frac{E_2}{RT^H(Y)}\right)\left(-Yf_1\left(T^H(Y)\right) + (1-Y)f_2\left(T^H(Y)\right)\right)\right] , \end{aligned} \tag{56}$$

with $\chi = \dfrac{Q}{RT^H(Y)} + 2\left(\beta - 1 + \dfrac{E_1}{RT^H(Y)}\right)$.

In the endothermic domain, we know that $-Yf_1\left(T^H(Y)\right) + (1-Y)f_2\left(T^H(Y)\right) > 0$. Therefore, $g''(Y)$ will be proved to be positive if we show that:

$$\chi \geq 0 \ \text{ and } \ \chi_2^2 - \chi_2 - \frac{E_2}{RT^H(Y)} \geq 0 \ . \tag{57}$$

Regarding the second expression in (57) as a second-order polynomial in the variable χ_2, we can rewrite these two conditions as:

$$\frac{2E_1 + Q}{2RT^H(Y)} \geq 1 - \beta \ \text{ and } \ \chi_2 = \beta + \frac{E_2}{RT^H(Y)} \geq \frac{1}{2} + \sqrt{\frac{E_2}{RT^H(Y)} + \frac{1}{4}} \ . \tag{58}$$

After some simple algebra, using the assumption (41) on β, one easily checks that the last condition in (58) is equivallent to: $2RT^H(Y) \leq E_2$. Both conditions (58) are then fulfilled from (40), which ends the proof. •

Remark 4.6: It is easy to see from the above proof that the same conclusions can be reached even if $\beta < 0$, but with a stronger hypothesis than (40) on the activation energies. For instance, the above results remain true if the conditions (40)-(41) are replaced by:

$$\beta \geq -3 \ \text{ and } \ 2RT_{max} \leq \min\left(\frac{E_1 + E_2}{4} \ , \ \frac{E_2}{3}\right) \ . \bullet \tag{59}$$

Remark 4.7: In fact, the preceding proofs show that the CL method is unconditionally stable as soon as the initial condition satisfies $Y^0 \leq Y^*(T^0)$. Indeed, if the initial data lies above the curve $Y = Y^*(T)$ but in the exothermic domain, we know that $0 \leq Y^{n+1} \leq 1$ for any $\Delta t > 0$, and (50) shows that $Y^{n+1} < Y^n$. This means that the sequence (Y^n) is decreasing for n small enough. Then, either this sequence always decreases, which means that $(Y^n, T^n) \in \mathcal{R}_+$ and $Y^n < Y^*(T^n)$ for all n, and the scheme is unconditionally stable from Lemma 4.4; or there exists n_0 such that $(Y^{n_0}, T^{n_0}) \in \mathcal{R}_-$ and,

for $n > n_0$, the sequence (Y^n) increases but (Y^n, T^n) remains in the endothermic domain from Lemma 4.5. In both cases, we have:

$$\lim_{n \nearrow +\infty} Y^n = Y^\infty \ , \quad \lim_{n \nearrow +\infty} T^n = T^\infty \ . \bullet \tag{60}$$

To conclude our analysis, it remains to examine why the CL method is *not* unconditionally stable in the whole exothermic domain. This is the object of the next Lemma:

Lemma 4.8:
The coupled linearized method is not always unconditionnally stable for the simple reversible reaction (29). •

PROOF: In Lemma 4.4, we have written only a sufficient condition for the stability of the method. Now, returning to (46) and assuming that $0 \leq Y^n \leq 1$, it is easy to see that the property:

$$0 \leq Y^{n+1} \leq 1 \quad \forall \Delta t > 0 \tag{61}$$

is achieved if the following two *necessary and sufficient* conditions are satisfied:

$$\begin{cases} f_2(T^n) + UY^n \left(-Y^n f_1'(T^n) + (1-Y^n) f_2'(T^n)\right) \geq 0 \ , \\ \\ f_1(T^n) + U(1-Y^n) \left(-Y^n f_1'(T^n) + (1-Y^n) f_2'(T^n)\right) \geq 0 \ . \end{cases} \tag{62}$$

Writing the first inequality as $\Lambda_1(Y) = (f_1' + f_2')Y^2 - f_2' Y - \dfrac{f_2}{U} \leq 0$, we see that the discriminant of Λ_1, $\Delta(\Lambda_1) = f_2'^2 + \dfrac{4f_2}{U}(f_1' + f_2')$, is always positive, and that Λ_1 has exactly one positive root. The first condition in (62) may therefore be written under the form:

$$Y^n \leq \mathcal{Y}_1(T^n) \ . \tag{63}$$

With realistic values for E_1, Q and T (see Remark 4.1), $\Lambda_1(1)$ is positive, which means that $0 < \mathcal{Y}_1(T) < 1$ and that (63) introduces an actual restriction.

The second inequality in (62) leads to:

$$\Lambda_2(Y) = (f_1' + f_2')Y^2 - (2f_2' + f_1')Y + \frac{f_1}{U} + f_2' \geq 0 \ . \tag{64}$$

The discriminant of Λ_2 is $\Delta(\Lambda_2) = f_1'^2 - \dfrac{4f_1}{U}(f_1' + f_2')$. Again, with realistic values for E_1, Q and T, this expression is positive. Examining the values of $\Lambda_2(0)$, $\Lambda_2'(0)$, $\Lambda_2(1)$, $\Lambda_2'(1)$, it is easy to see that Λ_2 has two roots inside the interval $[0, 1]$, which means that the second condition in (62) is equivallent to a condition of the form:

$$Y^n \notin [\mathcal{Y}_2(T^n), \mathcal{Y}_3(T^n)] \ , \tag{65}$$

with $0 < \mathcal{Y}_2(T) < \mathcal{Y}_3(T) < 1$.

The two conditions (63)-(65) show that the CL scheme is not unconditionally stable. •

We will not try to exploit any further the conditions (63)-(65), which are quite heavy to handle with. Instead, we will now examine the simpler case of a non-reversible reaction.

4.2 The one-step reaction

For the sake of simplicity, let us now consider the simplest case of a single one-step reaction $A \longrightarrow B$. Keeping the same notations as above, we will simply assume that $A_2 = 0$ in (31). Our aim here is to compare the stability restrictions for the linearized implicit schemes and the first-order explicit scheme.

We easily have:

$$Y^{n+1} = Y^n \left(1 - \Delta t f_1(T^n)\right) \tag{66}$$

for the explicit forward Euler scheme,

$$Y^{n+1} = \frac{Y^n}{1 + \Delta t f_1(T^n)} \tag{67}$$

for the UL method, which is still unconditionally stable, and:

$$Y^{n+1} = \frac{\dfrac{Y^n}{\Delta t} - U(Y^n)^2 f_1'(T^n)}{\dfrac{1}{\Delta t} + f_1(T^n) - UY^n f_1'(T^n)} \tag{68}$$

for the CL scheme. It is then easy to see that the explicit method (66) is stable under the condition:

$$\Delta t \leq \Delta t_{EXP} = \frac{1}{f_1(T^n)} \ , \tag{69}$$

whereas the CL method is stable under the following condition (if $Y^n > 0$):

$$\Delta t \leq \Delta t_{CL} = \frac{1}{UY^n f_1'(T^n)} \ . \tag{70}$$

Then, the ratio of these two limiting values of the time step is:

$$\frac{\Delta t_{CL}}{\Delta t_{EXP}} = \frac{f_1(T^n)}{UY^n f_1'(T^n)} = \frac{T^n}{T_{max} - T_{min}} \ \frac{1}{Y^n} \ \frac{1}{\beta + \dfrac{E_1}{RT^n}} \ ; \tag{71}$$

we have used Remark 4.1 and (48). It is then clear that this ratio can be substantially smaller than 1: *the stability restriction of the coupled linearized implicit method is then strictly more severe than the stability limit of the explicit Euler forward scheme !!*

4.3 Global hydrogen-oxygen reactions

We will now analyse further the UL method, which we found to be unconditionnally stable for the simple reversible model (29), for two global formulations of the hydrogen-oxygen combustion. In fact, we will consider the two following reversible models:

$$2H_2 + O_2 \rightleftharpoons 2H_2O \ , \tag{72}$$

and:

$$H_2 + \frac{1}{2}O_2 \rightleftharpoons H_2O \ , \tag{73}$$

and we will show that, surprisingly, the application of the uncoupled linearized method to (72) and (73) leads to very different stability limits.

4.3.1 The model with integer stoechiometric coefficients

Let us begin with the first model (72).

Calling X, Y and Z the mass fractions of H_2, O_2 and H_2O respectively, and $f_1(T)$ and $f_2(T)$ the forward and reverse reaction rates, we are led to the system:

$$\left\{ \begin{array}{l} \dot{X} = -2W_{H_2} \left(X^2 Y f_1 - Z^2 f_2\right) \ , \\ \dot{Y} = -W_{O_2} \left(X^2 Y f_1 - Z^2 f_2\right) \ , \\ \dot{Z} = 2W_{H_2O} \left(X^2 Y f_1 - Z^2 f_2\right) \ . \end{array} \right. \tag{74}$$

We then have the following result:

Proposition 4.9:
For the global reversible reaction (72), *the uncoupled linearized method is unconditionnally stable: if* X^n, Y^n, $Z^n \geq 0$ *and* $X^n + Y^n + Z^n = 1$, *then* X^{n+1}, Y^{n+1}, $Z^{n+1} \geq 0$ *and* $X^{n+1} + Y^{n+1} + Z^{n+1} = 1$ *for any* Δt. •

PROOF: Writing $\delta F = F^{n+1} - F^n$ for $F = X$, Y or Z, we may write the UL method for the mass fraction X as:

$$\frac{\delta X}{\Delta t} = -2W_{H_2}\left[\left(X^2Yf_1 - Z^2f_2\right) + 2XYf_1\delta X + X^2f_1\delta Y - 2Zf_2\delta Z\right] \ . \tag{75}$$

We have omitted the superscripts n for X^n, Y^n and Z^n in the right-hand side of this relation. Moreover, we have $\delta Y = \dfrac{W_{O_2}}{2W_{H_2}}\delta X$ and $\delta Z = -\dfrac{W_{H_2O}}{W_{H_2}}\delta X$ from (74). After a straightforward calculation, we obtain:

$$\left\{\begin{array}{l} X^{n+1} = \dfrac{\dfrac{X}{\Delta t} + \left(W_{O_2}X^3 + 2W_{H_2}X^2Y\right)f_1 + \left(4W_{H_2O}XZ + 2W_{H_2}Z^2\right)f_2}{\dfrac{1}{\Delta t} + \left(4W_{H_2}XY + W_{O_2}X^2\right)f_1 + 4W_{H_2O}Zf_2}, \\ \\ Y^{n+1} = \dfrac{\dfrac{Y}{\Delta t} + 4W_{H_2}XY^2f_1 + \left(4W_{H_2O}YZ + W_{O_2}Z^2\right)f_2}{\dfrac{1}{\Delta t} + \left(4W_{H_2}XY + W_{O_2}X^2\right)f_1 + 4W_{H_2O}Zf_2}, \\ \\ Z^{n+1} = \dfrac{\dfrac{Z}{\Delta t} + \left(2W_{H_2O}X^2Y + W_{O_2}X^2Z + 4W_{H_2}XYZ\right)f_1 + \left(2W_{H_2O}Z^2\right)f_2}{\dfrac{1}{\Delta t} + \left(4W_{H_2}XY + W_{O_2}X^2\right)f_1 + 4W_{H_2O}Zf_2} \ . \end{array}\right. \tag{76}$$

Now, assume that X^n, Y^n, $Z^n \geq 0$ and that $X^n + Y^n + Z^n = 1$. It is then obvious that X^{n+1}, Y^{n+1}, $Z^{n+1} \geq 0$ for any $\Delta t > 0$. Moreover, using the relation $2W_{H_2} + W_{O_2} = 2W_{H_2O}$, it is easy to check that $X^{n+1} + Y^{n+1} + Z^{n+1} = 1$, which completes the proof. •

4.3.2 The model with non-integer stoechiometric coefficients

Considering now the second model (73) and using the same notations, we obtain the system:

$$\left\{\begin{array}{l} \dot{X} = -W_{H_2}\left(X\sqrt{Y}f_1 - Zf_2\right) \ , \\ \\ \dot{Y} = -\dfrac{W_{O_2}}{2}\left(X\sqrt{Y}f_1 - Zf_2\right) \ , \\ \\ \dot{Z} = W_{H_2O}\left(X\sqrt{Y}f_1 - Zf_2\right) \ . \end{array}\right. \tag{77}$$

We then have the following result, which says that the UL method is *not* unconditionnally stable for this model:

Proposition 4.10:
For the global reversible reaction (73), *the uncoupled linearized method is not unconditionally stable. The stability condition writes:*

$$\frac{1}{\Delta t} \geq \left(\frac{W_{O_2}X}{4\sqrt{Y}} - W_{H_2}\sqrt{Y}\right)f_1 - \left(\frac{W_{O_2}Z}{2Y} + W_{H_2O}\right)f_2 \ , \tag{78}$$

for $Y > 0$. •

PROOF: After some algebra, we find that the application of the UL method to (77) leads to:

$$\left\{ \begin{array}{l} X^{n+1} = \dfrac{\dfrac{X}{\Delta t} + \dfrac{X^2 W_{O_2}}{4\sqrt{Y}} f_1 + \left(X W_{H_2O} + Z W_{H_2}\right) f_2}{\dfrac{1}{\Delta t} + \left(W_{H_2}\sqrt{Y} + \dfrac{W_{O_2} X}{4\sqrt{Y}}\right) f_1 + W_{H_2O} f_2} \ , \\ \\ Y^{n+1} = \dfrac{\dfrac{Y}{\Delta t} + \left(W_{H_2} Y\sqrt{Y} - \dfrac{W_{O_2} X\sqrt{Y}}{4}\right) f_1 + \left(W_{H_2O} Y + \dfrac{Z W_{O_2}}{2}\right) f_2}{\dfrac{1}{\Delta t} + \left(W_{H_2}\sqrt{Y} + \dfrac{W_{O_2} X}{4\sqrt{Y}}\right) f_1 + W_{H_2O} f_2} \ , \\ \\ Z^{n+1} = \dfrac{\dfrac{Z}{\Delta t} + \left(Z\sqrt{Y} W_{H_2} + \dfrac{W_{O_2} XZ}{4\sqrt{y}} + X\sqrt{Y} W_{H_2O}\right) f_1}{\dfrac{1}{\Delta t} + \left(W_{H_2}\sqrt{Y} + \dfrac{W_{O_2} X}{4\sqrt{Y}}\right) f_1 + W_{H_2O} f_2} \ . \end{array} \right. \tag{79}$$

The arguments are then the same as in the preceding proof: assuming that X^n, Y^n, $Z^n \geq 0$ and that $X^n + Y^n + Z^n = 1$, it is obvious that, for any $\Delta t > 0$, we have $X^{n+1} \geq 0$, $Z^{n+1} \geq 0$ and $X^{n+1} + Y^{n+1} + Z^{n+1} = 1$. Also, it is clear that $Y^{n+1} \geq 0$ if and only if (78) holds, which completes the proof. •

Remark 4.11: Let us comment about the stability condition (78). It is clear that, if X is small enough, i.e. for sufficiently *lean* mixtures, the UL scheme is unconditionnally stable (the right-hand side of (78) is then negative). On the other hand, for *rich* mixtures, i.e for Y small enough, there is an actual limitation on Δt, which takes the form (at the leading order):

$$\Delta t \leq \Delta t_{UL} = \frac{4\sqrt{Y}}{X W_{O_2} f_1} \ . \tag{80}$$

On the other hand, it is readily seen in this case that the stability limit of the explicit forward Euler scheme reads:

$$\Delta t \leq \Delta t_{EXP} = \frac{2\sqrt{Y}}{X W_{O_2} f_1} \ . \tag{81}$$

Thus, for very rich mixtures, the uncoupled linearized method may operate with time steps which are only twice greater than the time step allowed for the explicit method. •

4.4 A remark about the fractional-step approach

The previous sections show on the basis of the analysis of several tractable models that the linearized implicit methods suffer from very severe stability restrictions for the integration of the chemical model (8). One may then wonder whether this result is not due, at least partly, to our fractional-step approach. In other words, may the linearized implicit schemes operate with larger time steps if, instead of considering the sole chemical source terms, we simultaneously integrate the convective (and possibly the diffusive) terms together with the chemical terms ?

The answer to this question is negative: the stability limit of the linearized implicit methods for the coupled convective-reactive system is not any greater than the stability limit of these schemes for the purely chemical system (8). This fact is illustrated by the following example, where we consider the most simple convective-reactive system for a one-step reaction $A \longrightarrow B$, with constant velocity and constant energy:

$$Y_t + u_0 Y_x = -Y f_1(H^0 - UY) \ . \tag{82}$$

Assuming for the sake of clarity that $u_0 > 0$ and setting again $T^H(Y) = H^0 - UY$, we have (compare with (70)):

Lemma 4.12:
For the solution of (82), the upwind linearized implicit scheme:

$$\frac{Y_j^{n+1} - Y_j^n}{\Delta t} + u_0 \frac{Y_j^{n+1} - Y_{j-1}^{n+1}}{\Delta x} = -Y_j^{n+1} f_1\left(T^H(Y_j^n)\right) + UY_j^n f_1'\left(T^H(Y_j^n)\right)\left(Y_j^{n+1} - Y_j^n\right) \tag{83}$$

is stable under the condition:

$$\Delta t \leq \frac{1}{\max_j UY_j^n f_1'\left(T^H(Y_j^n)\right)} \ . \bullet \tag{84}$$

PROOF: The scheme (83) can be written in matrix form as $\mathcal{A}Y^{n+1} = \mathcal{B}Y^n$, with:

$$\mathcal{A}_{j,j} = \frac{1}{\Delta t} + f_1\left(H^0 - UY_j^n\right) - UY_j^n f_1'\left(H^0 - UY_j^n\right) + \frac{u_0}{\Delta x} \ , \quad \mathcal{A}_{j,j-1} = -\frac{u_0}{\Delta x} \ , \tag{85}$$

$$\mathcal{B}_{j,j} = \frac{1}{\Delta t} - UY_j^n f_1'\left(H^0 - UY_j^n\right) \ , \tag{86}$$

all other terms being zero. Clearly, if (84) holds, then $\mathcal{B} \geq 0$, and $\mathcal{A}$ is an M-matrix ($\mathcal{A}_{j,j} > 0$ for all j, $\mathcal{A}_{j,k} \leq 0$ for $j \neq k$ and $\sum_k \mathcal{A}_{j,k} > 0$ for all j; see [11]). As a consequence, $\mathcal{A}^{-1} \geq 0$, whence $Y^{n+1} \geq 0$ as soon as $Y^n \geq 0$.

If (84) holds, we may also set $\mathcal{C} = \mathcal{B}^{-1}\mathcal{A}$ and write the scheme (83) as $\mathcal{C}Y^{n+1} = Y^n$. Then, $\mathcal{C}$ is an M-matrix and, denoting 1 the vector whose components are all equal to unity, we easily see that $\mathcal{C}1 \geq 1$. Thus, $\mathcal{C}^{-1} \geq 0$ and we have $\mathcal{C}^{-1}1 \leq 1$. Assuming that $Y^n \leq 1$, we see that $Y^{n+1} = \mathcal{C}^{-1}Y^n \leq 1$, which ends the proof: the inequalities $0 \leq Y_j^{n+1} \leq 1$ hold for all j. •

5 Conclusions

We have investigated in this paper the use of the nonlinear implicit and linearized implicit methods for the time integration of exothermic complex chemistry models.

We have enlightened the inefficiency of these methods through three numerical experiments, which showed *(i)* that a straightforward use of these methods leads to prohibitive computation times for the simulation of hydrogen combustion, *(ii)* that, for some initial conditions, several of these methods are unable to preserve the mass fractions positivity, even with extremely small time steps, and, more importantly and more surprisingly, *(iii)* that monitoring the time step for these calculations by only requiring the preservation of the mass fractions positivity may lead to physically unacceptable results.

We explained these observations by analysing the behaviour of the linearized implicit methods for several (not too complex) tractable chemical mechanisms. These analyses show that the stability limit of the linearized implicit methods strongly depend on the detailed form of the chemical model. Also, they explain in a convincing way that the linearized implicit methods are not suitable for the time integration of exothermic chemical mechanisms, whereas they are known to be adequate for endothermic chemistries (see [2, 3, 8]).

Remark 5.1: The nonlinear implicit methods deserve some further comments. Following the arguments used in [4], it can indeed be shown that, for any time step Δt, as soon as the nonlinear discrete system to be solved in these methods has a solution $(Y_k)^{n+1}$, T^{n+1}, then this solution satisfies the maximum principle: $0 \leq Y_k^{n+1} \leq 1$ (and this remains true if convective and diffusive terms are added; see [4]). Therefore, the instabilities observed for these methods in our experiments should be interpreted as the divergence of the Newton iterations for the solution of the nonlinear discrete problem, not as an intrinsic instability of the nonlinear formulation itself. It might in fact be the case that this situation can be

improved by using another iterative technique instead of Newton method (such as damped Newton, GMRES, ...), or by coupling the convective or diffusive terms with the chemical source terms within the iterations (see e.g. [10]). •

APPENDIX A

We give here the expression of the Jacobian matrix of the chemical terms.

Using the notations of Section 3.1, we wish to evaluate $G = \dfrac{\partial \mathcal{C}}{\partial X}$. We first obtain:

$$\frac{\partial \mathcal{C}_1}{\partial T}|_{Y_k} = \sum_{k=1}^{\kappa} Y_k C_{v_k}(T) \ , \quad \frac{\partial \mathcal{C}_1}{\partial Y_k}|_{T, Y_{m\ (m \neq k)}} = \epsilon_k(T) \ .$$

For $k \geq 0$, we have:

$$\frac{\partial \mathcal{C}_{k+1}}{\partial T}|_{Y_m} = -W_k \ \Delta t \ \sum_{i=1}^{I} \nu_{ki} \frac{\partial \mathcal{R}_i}{\partial T}|_{N_m} \ ,$$

with:

$$\frac{\partial \mathcal{R}_i}{\partial T}|_{N_m} = B_i \ \left[K_{f,i} \prod_{k=1}^{\kappa} N_k^{\nu'_{ki}} \left(\frac{\beta_i}{T} + \frac{E_i}{R_c T^2} \right) \right.$$

$$\left. - K_{r,i} \prod_{k=1}^{\kappa} N_k^{\nu''_{ki}} \left(\frac{\beta_i + \Delta\nu_i}{T} + \frac{E_i}{R_c T^2} - \sum_{k=1}^{\kappa} \nu_{ki} \ \mathcal{G}_k(T) \right) \right] \ ,$$

$$N_k = \frac{\rho Y_k}{W_k} \ , \quad B_i = \sum_{k=1}^{\kappa} \alpha_{ki} N_k \ ,$$

$$\mathcal{G}_k(T) = \frac{a_{6k}}{T^2} + \frac{a_{1k}}{T} + \frac{a_{2k}}{2} + \frac{a_{3k}}{3} T + \frac{a_{4k}}{4} T^2 + \frac{a_{5k}}{5} T^3 \ ,$$

$$h_k(T) = \frac{R}{W_k} \left(\ a_{6k} + a_{1k} T + \frac{a_{2k}}{2} T^2 + \frac{a_{3k}}{3} T^3 + \frac{a_{4k}}{4} T^4 + \frac{a_{5k}}{5} T^5 \ \right) \ ,$$

$$C_{pk}(T) = \frac{d}{dT} h_k(T) = \frac{R}{W_k} \left(\ a_{1k} + a_{2k} T + a_{3k} T^2 + a_{4k} T^3 + a_{5k} T^4 \ \right) \ ,$$

$$C_{vk}(T) = \frac{d}{dT} \epsilon_k(T) = C_{pk}(T) - \frac{R}{W_k} \ .$$

Lastly, we have (δ_{km} denoting the Kronecker delta):

$$\frac{\partial \mathcal{C}_{k+1}}{\partial Y_m}|_{T, Y_{l\ (l \neq m)}} = \delta_{km} - \Delta t \ W_k \sum_{i=1}^{I} \nu_{ki} \frac{\partial \mathcal{R}_i}{\partial Y_m}|_{T, Y_{l\ (l \neq m)}} \ ,$$

with :

$$\frac{\partial \mathcal{R}_i}{\partial Y_m}|_{T, Y_{l\ (l \neq m)}} = \frac{\rho \alpha_{mi} \mathcal{R}_i}{W_m B_i} + B_i \ \left(K_{f,i} \prod_{l \neq m} N_l^{\nu'_{li}} \frac{\rho \nu'_{mi}}{W_m} N_m^{\nu'_{mi}-1} - K_{r,i} \prod_{l \neq m} N_l^{\nu''_{li}} \frac{\rho \nu''_{mi}}{W_m} N_m^{\nu''_{mi}-1} \right) \ .$$

In the case of chemical reactions not including a colliding third body, the above expressions are still valid with $B_i = 1$ and removing the terms involving α_{mi} in the last relation.

APPENDIX B

We now write down the two hydrogen-air combustion models, in CHEMKIN format (i.e. with C.G.S. units, activation energies E_i in $cal.mol^{-1}$).

The model with 9 species and 19 reactions writes:

				A_i	β_i	E_i
1	$H_2 + O_2$	$\rightleftharpoons$	$2OH$	$1.70E13$	$0.$	$47780.$
2	$H_2 + OH$	$\rightleftharpoons$	$H_2O + H$	$1.17E09$	1.3	$3626.$
3	$H + O_2$	$\rightleftharpoons$	$OH + O$	$5.13E16$	-0.816	$16507.$
4	$O + H_2$	$\rightleftharpoons$	$OH + H$	$1.80E10$	$1.$	$8826.$
5	$H + O_2 + M$	$\rightleftharpoons$	$HO_2 + M$	$2.10E18$	$-1.$	$0.$
6	$H + O_2 + O_2$	$\rightleftharpoons$	$HO_2 + O_2$	$6.70E19$	-1.42	$0.$
7	$H + O_2 + N_2$	$\rightleftharpoons$	$HO_2 + N_2$	$6.70E19$	-1.42	$0.$
8	$OH + HO_2$	$\rightleftharpoons$	$H_2O + O_2$	$5.00E13$	$0.$	$1000.$
9	$H + HO_2$	$\rightleftharpoons$	$2OH$	$2.50E14$	$0.$	$1900.$
10	$O + HO_2$	$\rightleftharpoons$	$O_2 + OH$	$4.80E13$	$0.$	$1000.$
11	$2OH$	$\rightleftharpoons$	$O + H_2O$	$6.00E08$	1.3	$0.$
12	$H_2 + M$	$\rightleftharpoons$	$2H + M$	$2.23E12$	0.5	$92600.$
13	$O_2 + M$	$\rightleftharpoons$	$2O + M$	$1.85E11$	0.5	$95560.$
14	$H + OH + M$	$\rightleftharpoons$	$H_2O + M$	$7.50E23$	-2.6	$0.$
15	$H + HO_2$	$\rightleftharpoons$	$H_2 + O_2$	$2.50E13$	$0.$	$700.$
16	$2HO_2$	$\rightleftharpoons$	$H_2O_2 + O_2$	$2.00E12$	$0.$	$0.$
17	$H_2O_2 + M$	$\rightleftharpoons$	$2OH + M$	$1.30E17$	$0.$	$45500.$
18	$H_2O_2 + H$	$\rightleftharpoons$	$HO_2 + H_2$	$1.60E12$	$0.$	$3800.$
19	$H_2O_2 + OH$	$\rightleftharpoons$	$H_2O + HO_2$	$1.00E13$	$0.$	$1800.$

For reactions 5, 12 and 14, the third-body-efficiency coefficients of α_{ki}'s are given by:

$$\alpha_{H_2O,5} = 21 \ , \quad \alpha_{H_2,5} = 3.3 \ ,$$

$$\alpha_{H_2O,12} = 6 \ , \quad \alpha_{H,12} = 2 \ , \quad \alpha_{H_2,12} = 3 \ ,$$

$$\alpha_{H_2O,14} = 20 \ .$$

The model with 10 species and 16 reactions is the following:

				A_i	β_i	E_i
1	$H_2 + O_2$	$\rightleftharpoons$	$2OH$	$1.70E13$	$0.$	$47780.$
2	$H_2 + OH$	$\rightleftharpoons$	$H_2O + H$	$5.20E13$	0.0	$6500.$
3	$H + O_2$	$\rightleftharpoons$	$OH + O$	$1.22E17$	-0.907	$16620.$
4	$O + H_2$	$\rightleftharpoons$	$OH + H$	$1.80E10$	$1.$	$8826.$
5	$H + O_2 + M$	$\rightleftharpoons$	$HO_2 + M$	$2.00E15$	$0.$	$-870.$
6	$OH + HO_2$	$\rightleftharpoons$	$H_2O + O_2$	$1.20E13$	$0.$	$0.$
7	$H + HO_2$	$\rightleftharpoons$	$2OH$	$6.00E13$	$0.$	$0.$
8	$O + HO_2$	$\rightleftharpoons$	$O_2 + OH$	$1.00E13$	$0.$	$0.$
9	$2OH$	$\rightleftharpoons$	$O + H_2O$	$1.70E06$	2.03	$-1190.$
10	$H_2 + M$	$\rightleftharpoons$	$2H + M$	$2.23E12$	0.5	$92600.$
11	$O_2 + M$	$\rightleftharpoons$	$2O + M$	$1.85E11$	0.5	$95560.$
12	$H + OH + M$	$\rightleftharpoons$	$H_2O + M$	$7.50E23$	-2.6	$0.$
13	$H + HO_2$	$\rightleftharpoons$	$H_2 + O_2$	$1.30E13$	$0.$	$0.$
14	$O + N_2$	$\rightleftharpoons$	$NO + N$	$1.40E14$	$0.$	$75800.$
15	$N + O2$	$\rightleftharpoons$	$NO + O$	$6.40E09$	$1.$	$6280.$
16	$OH + N$	$\rightleftharpoons$	$NO + H$	$4.00E13$	$0.$	$0.$

For reactions 5, 10 and 12, the third-body-efficiency coefficients of α_{ki}'s are given by:

$$\alpha_{H_2O,5} = 20 \ , \quad \alpha_{H_2O,10} = 5 \ , \quad \alpha_{H_2O,12} = 20 \ .$$

APPENDIX C

Lastly, we give here the FORTRAN Routine for Gill's Runge-Kutta 2 method, taken from [12].

```
      SUBROUTINE GILLS(N,C,F,X,H,M,K)
C
C   THIS ROUTINE PERFORMS RK CALCULATION BY GILLS METHOD
C
C  INPUT
C       N = NUMBER OF VARIABLES
C       C = ARRAY OF N DEPENDENT VARIABLES
C       F = ARRAY OF N DERIVATIVES OF C W.R.T. X
C       X = INDEPENDENT VARIABLE
C       H = INCREMENT OF X
C       M = INDEX USED IN THE ROUTINE (INITIALIZED TO ZERO
C           BEFORE THE FIRST CALL)
C  OUTPUT
C       X,C
C       K = TEST INTEGER
C         = 1 CONTINUE
C         = 2 RETURN
      IMPLICIT REAL*8 (A-H,O-Z)
      DIMENSION  C(10),F(10),Q(10)
      ONESIX = 1.D0/6.D0
      ONETHI = 1.D0/3.D0
      M = M +1
      GOTO(1,4,5,3,7),M
1     DO 2 I = 1,N
2     Q(I)= 0.D0
      A=0.5D0
      GOTO 9
3     A = 1.70710678118654752440D0
4     X = X + 0.5D0 * H
5     DO 6 I=1,N
      C(I) = C(I) + A * ( F(I)*H - Q(I) )
6     Q(I) = 2.D0 * A * H * F(I) + (1.D0 - 3.D0*A)*Q(I)
      A = 0.29289321881345247560D0
      GOTO 9
7     DO 8 I=1,N
8     C(I) = C(I) + H*F(I)*ONESIX - Q(I) * ONETHI
      M=0
      K=2
      GOTO 10
9     K=1
10    RETURN
      END
```

References

[1] Y. D'ANGELO, "Simulation numérique de phénomènes liés à la combustion supersonique", Thèse, ENPC, Paris, (1994).

[2] J. A. DESIDERI, N. GLINSKY & E. HETTENA, "Hypersonic reactive flow computation", *Comp. Fluids*, **18**, (2), pp. 151-182, (1990).

[3] J. A. DESIDERI, N. GLINSKY & L. FEZOUI, "Numerical computation of the chemical dissociation and relaxation phenomena behind a detached strong shock , INRIA Report 774, (1987).

[4] M. GHILANI & B. LARROUTUROU, "Upwind computation of steady planar flames with complex chemistry", Mod. Math. Anal. Num., **25**, (1), pp. 67-92, (1991).

[5] A. C. HINDMARSH, "ODEPACK, a systematized collection of ODE solvers", *IMACS Trans. on Sc. Comp.*, Stepleman et al. eds., pp. 55-64, North-Holland, Amsterdam, (1983).

[6] R. J. KEE, J. A. MILLER & T. H. JEFFERSON. "CHEMKIN: a general purpose, problem-independent, transportable, FORTRAN chemical kinetics code package", SANDIA Report SAND83-8209, (1983).

[7] B. LARROUTUROU, "How to preserve mass fractions positivity when computing compressible multi-component flows", *J. Comp. Phys.*, **95**, (1), pp. 59-84, (1991).

[8] C. P. LI, "Implicit methods for computing chemically reacting flows", NASA Techn. Mem. 58274, Houston, (1986).

[9] L. R. PETZOLD, "A Description of DASSL: a differential/algebraic system solver", *IMACS Trans. on Sc. Comp.*, Stepleman et al. eds., North-Holland, Amsterdam, (1983).

[10] M. D. SMOOKE, A. A. TURNBULL, R. E. MITCHELL & D. E. KEYES, "Solution of two-dimensional axisymmetric laminar diffusion flames by adaptive boundary value methods", *Mathematical modelling in combustion and related topics*, Brauner & Schmidt-Lainé eds., pp. 261-300, NATO ASI Series E, Nijhoff, Doordrecht, (1988).

[11] R. S. VARGA, "Matrix iterative analysis", Prentice Hall, (1962).

[12] F. M. WHITE, "Viscous fluid flow", (second edition), McGraw-Hill, New-York, (1991).

Contents